Random Thoughts on Heavy Flavor

R. Vogt

Physics Division, Lawrence Livermore National Laboratory
Physics Department, University of California at Davis

Quarkonium Production Issues

Numerous Production Models

Color Evaporation Model (CEM):

Hadronization scale $k = \mathcal{O}(\Lambda_{\rm QCD})$, $Q\overline{Q}$ quantum numbers changed by soft interactions with probabilities specific to each state but independent of energy (Barger *et al.*; Gavai *et al.*; Schuler and RV)

Color Singlet Model I (CSM):

$k = \mathcal{O}(m_Q)$, singlet states with correct quantum numbers; hard gluon needed for S states, *e.g.* $gg \to J/\psi g$; $gg \to \chi_{c2}$ dominant? (Baier *et al.*; Schuler)

Nonrelativistic QCD (NRQCD) – alias Color Octet Model:

$k = \mathcal{O}(\alpha_s m_Q)$, $Q\overline{Q}$ quantum numbers changed via gluon emission at bound state momentum scale; corresponds to velocity $v = k/m_Q$ expansion; nonperturbative octet and singlet matrix elements fit to data (Braaten, Bodwin and Lepage; Cho and Leibovich; Beneke and Rothstein; Maltoni *et al.* $\cdots$)

Color Singlet Model II (CSM*):

$k = \mathcal{O}(\sqrt{\hat{s}})$, new contributions from heretofore neglected "s-channel cut" diagrams for S states (Lansberg *et al.*)

Comover Enhancement Scenario (CES):

$k = \mathcal{O}(1/\tau_{\rm AP})$, $1/m_Q \leq \tau_{\rm AP} \leq 1/\Lambda_{\rm QCD}$, $Q\overline{Q}$ quantum numbers changed by perturbative interactions with comoving color field (Hoyer and Peigne)

Intrinsic Charm:

k typically assumed to be soft, $gc \to J/\psi c$ provides additional source of high p_T, forward J/ψ production (Brodsky and Lansberg)

Color Evaporation Model

All quarkonium states are treated like $Q\overline{Q}$ ($Q = c, b$) below $H\overline{H}$ ($H = D, B$) threshold

Distributions for all quarkonium family members identical. Production ratios should also be independent of $\sqrt{s}$, p_T, x_F.

At LO, $gg \to Q\overline{Q}$ and $q\overline{q} \to Q\overline{Q}$; NLO add $gq \to Q\overline{Q}q$

$$\sigma_Q^{\rm CEM} = F_Q \sum_{i,j} \int_{4m_Q^2}^{4m_H^2} d\hat{s} \int dx_1 dx_2 \; f_{i/p}(x_1, \mu^2) \; f_{j/p}(x_2, \mu^2) \; \hat{\sigma}_{ij}(\hat{s}) \; \delta(\hat{s} - x_1 x_2 s)$$

Values of m_Q and Q^2 fixed from NLO calculation of $Q\overline{Q}$ production

Data and branching ratios used to separate the F_Q's for each quarkonium state – $F_c = 1/9$ used in Amundson *et al.*

Gavai *et al.* fixed inclusive F_Q by comparison of NLO calculation of $\sigma_Q^{\rm CEM}$ to $\sqrt{s}$ dependence of J/ψ and Υ cross sections, $\sigma(x_F > 0)$ and $Bd\sigma/dy|_{y=0}$ for J/ψ, $Bd\sigma/dy|_{y=0}$ for Υ

Resonance	J/ψ	ψ'	χ_{c1}	χ_{c2}	Υ	Υ'	Υ''	$\chi_b(1P)$	$\chi_b(2P)$
$\sigma_i^{\rm dir}/\sigma_H$	**0.62**	**0.14**	**0.6**	**0.99**	**0.52**	**0.33**	**0.20**	**1.08**	**0.84**
f_i	**0.62**	**0.08**	**0.16**	**0.14**	**0.52**	**0.10**	**0.02**	**0.26**	**0.10**

Table 1: **The ratios of the direct quarkonium production cross sections, $\sigma_i^{\rm dir}$, to the inclusive J/ψ and Υ cross sections, denoted σ_H, and the feed down contributions of all states to the J/ψ and Υ cross sections, f_i, Digal *et al.*.**

Open and Hidden Charm Photo- and Hadroproduction Show Similar Energy Dependence

When normalization adjusted, the J/ψ and $D\overline{D}$ cross sections display similar energy dependencies in both photo- and hadroproduction

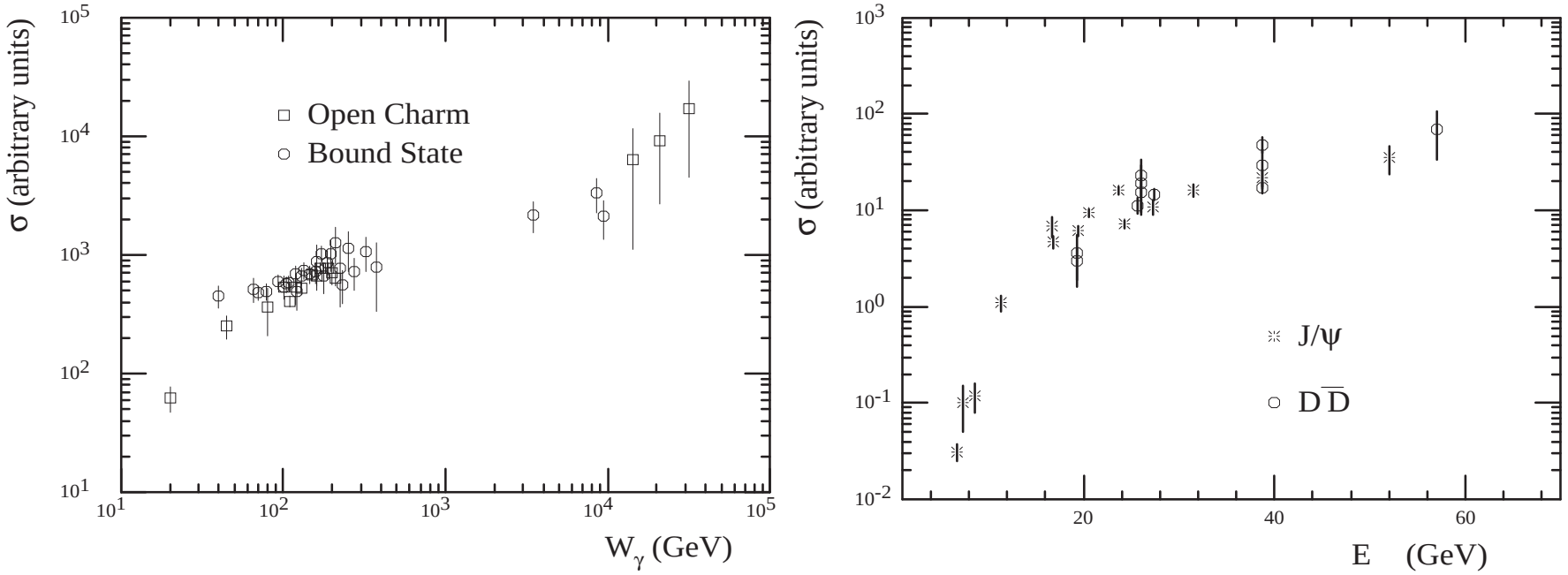

Figure 1: **(Left) Photoproduction data as a function of the photon energy in the hadron rest frame, W_γ. (Right) Hadroproduction data as a function of the center-of-mass energy, E_{cm}. In both cases, the normalization has been adjusted to show the similar shapes of the data.** [**Amundson** *et al.*]

CEM Total Cross Sections

Energy dependence of NLO CEM compared to photo- and hadroproduction data

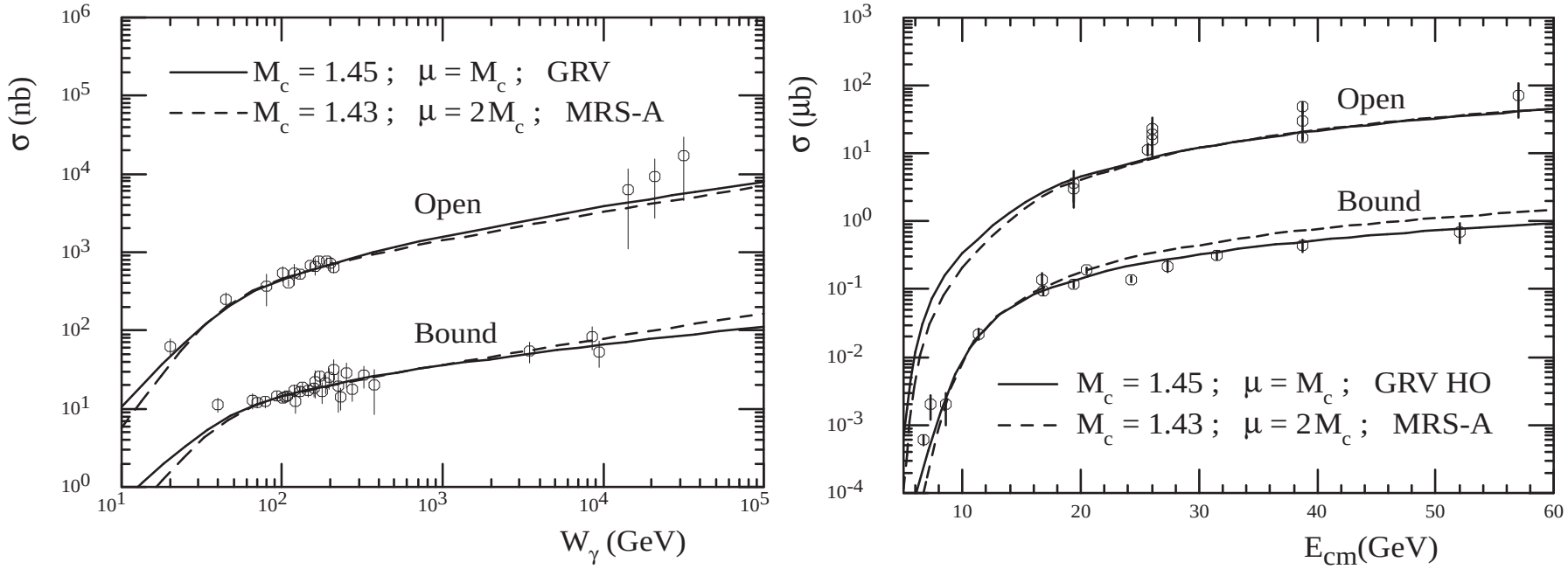

Figure 2: **(Left) Photoproduction data compared to NLO CEM predictions as a function of photon energy in the hadron rest from, W_γ. (Right) Hadroproduction data and the predictions of the CEM at NLO as a function of the center-of-mass energy, E_{cm}. The curve for bound state production is an absolutely normalized, parameter-free CEM prediction. [Amundson *et al.*]**

CDF Run I Data Shows Similar Charmonium p_T Dependence

High p_T Run I data show that, within uncertainties of the data, the prompt J/ψ, the ψ' and χ_c p_T dependencies are the same

Amundsen *et al.* calculated p_T distribution (only partial real part) harder than data at high p_T, undershoots at low p_T – likely because they do not include any k_T smearing

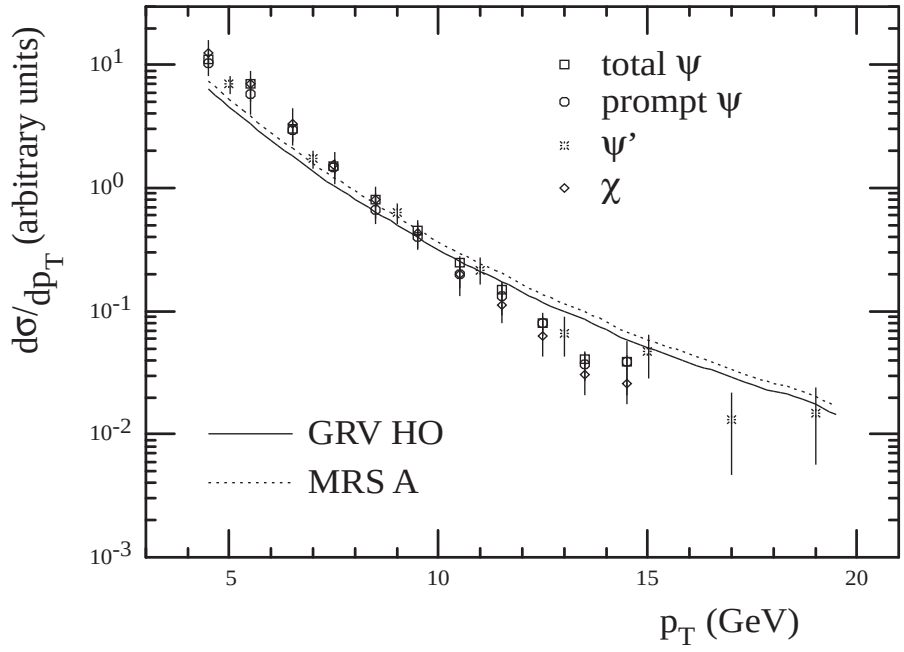

Figure 3: Run I data from the CDF Collaboration, shown with arbitrary normalization. The curves are the predictions of the color evaporation model at tree level, also shown with arbitrary normalization. The normalization is correctly predicted within a K-factor of 2.2. [From Amundsen *et al.*]

Comparison to CDF Run II Quarkonium Data

Complete calculation with $\langle k_T^2 \rangle = 2.53$ GeV^2 from high p_T Run I data may be too strong, $\langle k_T^2 \rangle = 1.76$ GeV^2 works better

Data may support even lower $\langle k_T^2 \rangle$ values, rather low average p_T for data

Normalization assumes inclusive J/ψ, no rapidity bin width included, scaled up to agree with total forward cross section

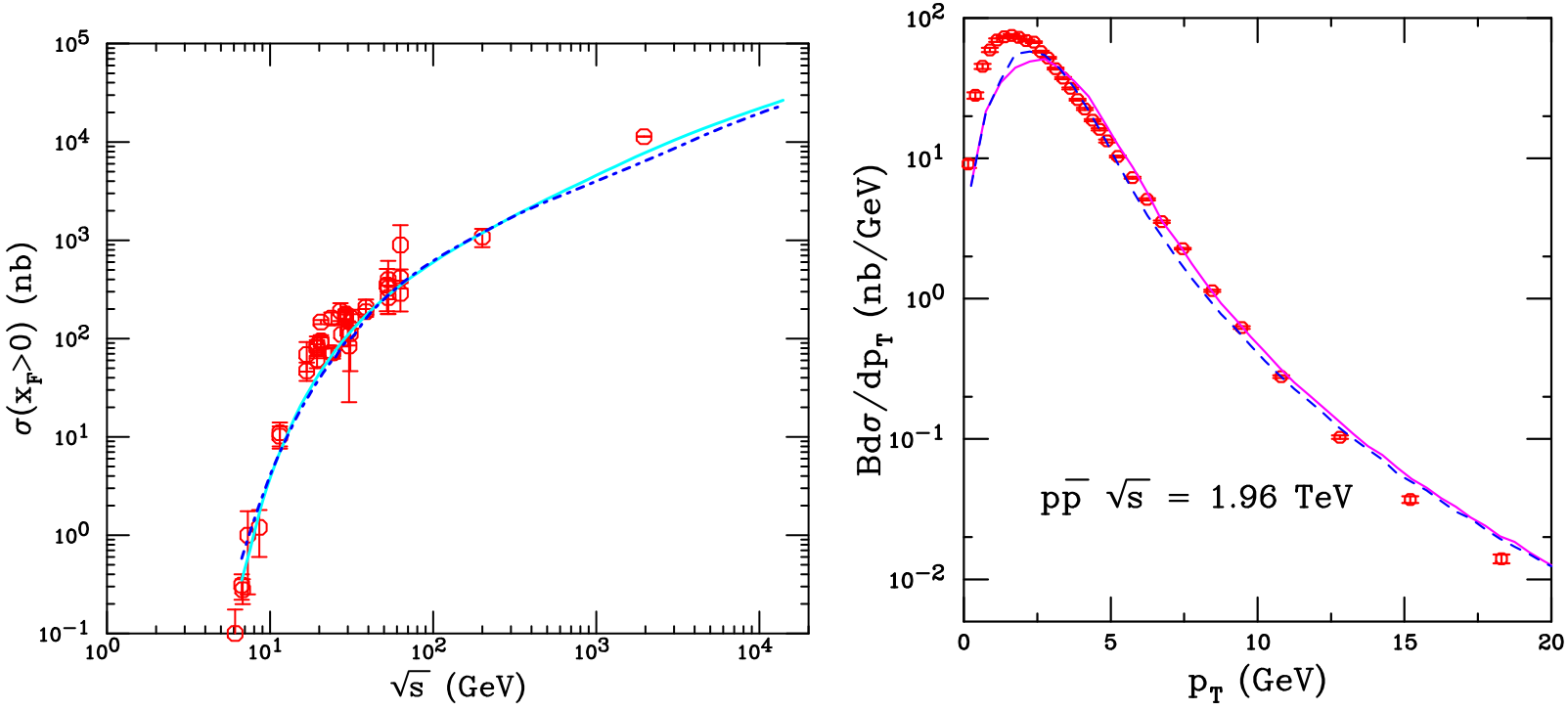

Figure 4: (Left) The J/ψ forward cross section calculated to NLO in the CEM. The solid cyan curve employs the MRST HO distributions while the dot-dashed blue curve is a result with CTEQ6M. Both take $m_c = 1.2$ GeV and $m_T = 2\sqrt{p_{T_{Q\overline{Q}}}^2 + m_c^2}$ for J/ψ. [After Phys. Rept. **458** (2008) 1.] (Right) The J/ψ p_T distributions compared to CDF data at $\sqrt{s} = 1.96$ TeV for $\langle k_T^2 \rangle = 2.53$ (solid magenta) and 1.76 (dashed blue) GeV^2. [After G. Schuler and R.V., Phys. Lett. B **387** (1996) 181.] There is an additional factor of 1.8 in the normalization to agree with the total cross section, assuming inclusive J/ψ and that the rapidity bin width is not included.

CEM Comparison to RHIC pp J/ψ Data

CEM calculation reproduces shape of J/ψ p_T and y distributions rather well
Normalization is also rather good, 'fudge' factor of 1.3 to match data

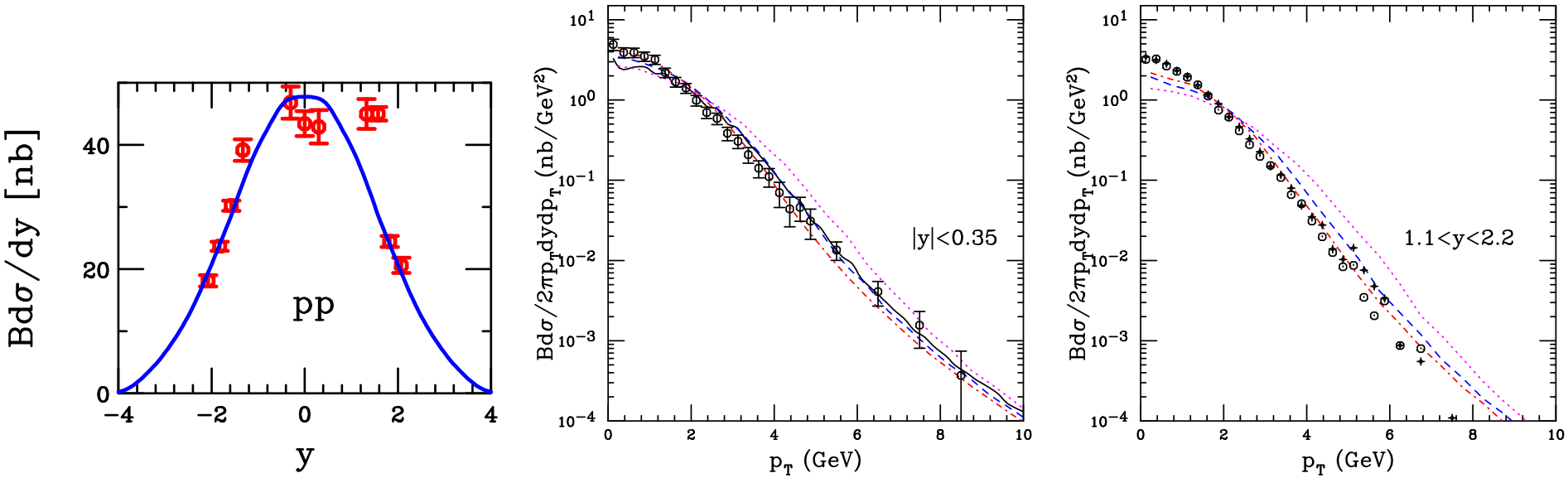

Figure 5: **PHENIX pp measurements compared to CEM calculation at $\sqrt{s} = 200$ GeV. The J/ψ rapidity distribution (left) and transverse momentum distributions at midrapidity (center) and in the muon arms (right). The solid black line in the center is a previous calculation with the MRST HO PDFs. The blue dashed, red dot-dashed and magenta dotted curves correspond to $\langle k_T^2 \rangle = 1.77$ GeV^2 (default kick), 1.38 GeV^2 (half default kick) and 2.53 GeV^2 (twice default kick).**

Why Intrinsic Charm?

Intrinsic Charm – $c\bar{c}$ pairs in the hadron wavefunction liberated by soft interactions – has been around a long time (Brodsky *et al.*)

Charm production seems to be anomalously large at high momentum fractions

- **EMC F_2^c large at higher x and Q^2**
- **Leading charm asymmetries in hadroproduction**
- **Large $pp \to \Lambda_c X$ production cross section at $x_F > 0.5$ (ISR)**
- **Double J/ψ production at high x_F in hadroproduction**

EMC (EMC, Hoffmann and Moore) result confirmed with NLO calculation of both extrinsic and intrinsic charm (Harris, Smith and R.V., Nucl. Phys. B461 (1996) 181)
HERA data on F_2^c is so far at too low x to check EMC

Extrinsic Charm $(\gamma^*(q) + a_1(k_1) \to c(p_1) + \overline{c}(p_2) + a_2(k_2))$

Structure function

$$F_2(x,Q^2,m_c^2) = \frac{Q^2\alpha_s(\mu^2)}{4\pi^2 m_c^2}\int_{\xi_{\min}}^1 \frac{d\xi}{\xi}\left[e_c^2 f_{g/p}(\xi,\mu^2)c_{2,g}^{(0)}\right] \frac{Q^2\alpha_s^2(\mu^2)}{\pi m_c^2}\int_{\xi_{\min}}^1 \frac{d\xi}{\xi}\left\{e_c^2 f_{g/p}(\xi,\mu_c^2)\left(c_{2,g}^{(1)} + \overline{c}_{2,g}^{(1)}\ln\frac{\mu^2}{m_c^2}\right)\right.$$
$$\left. + \sum_{i=q,\overline{q}} f_{i/p}(\xi,\mu^2)\left[e_c^2\left(c_{2,i}^{(1)} + \overline{c}_{2,i}^{(1)}\ln\frac{\mu^2}{m_c^2}\right) e_i^2\, d_{2,i}^{(1)} + e_c\, e_i\, o_{2,i}^{(1)}\right]\right\}$$

$\xi_{\min} = x(4m_c^2+Q^2)/Q^2$; c_i, d_i and o_i are scale-independent coefficient functions: c_i is for $\gamma^* c$ coupling, d_i for $\gamma^* q$ coupling, o is interference term

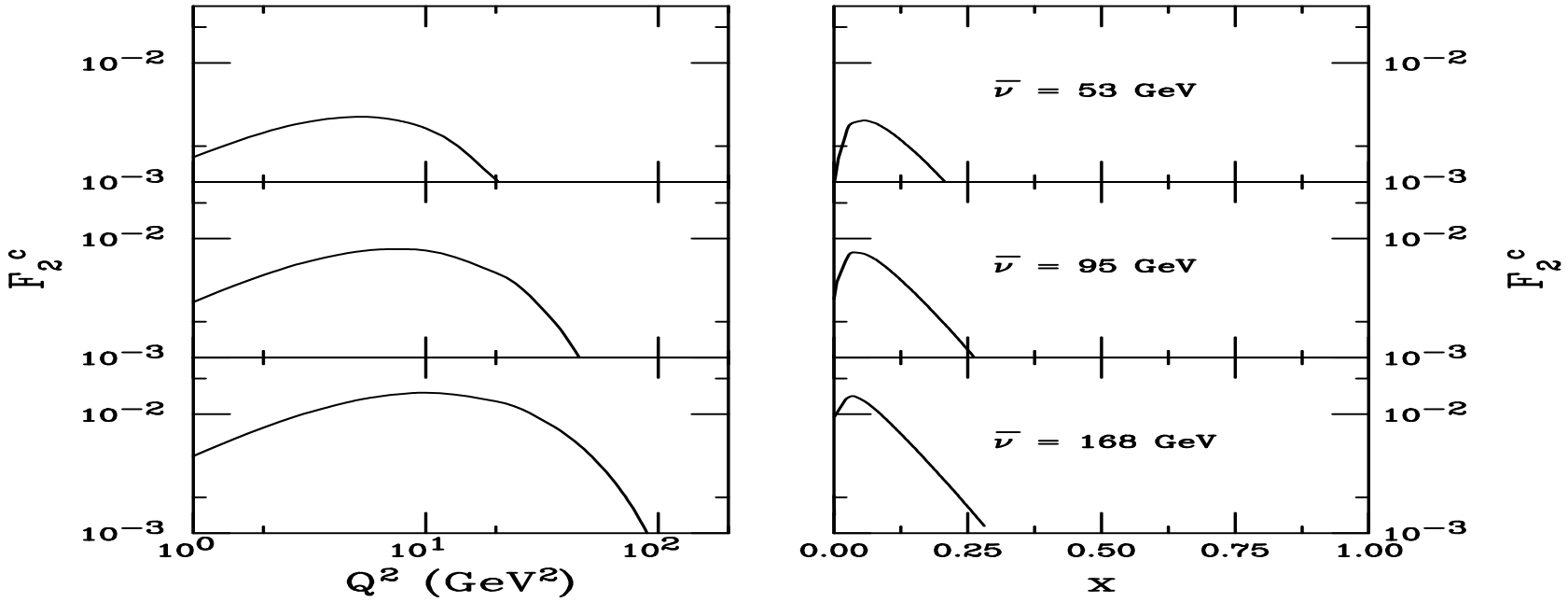

Figure 6: The extrinsic charm structure function used in the EMC analysis as a function of Q^2 (left-hand side) and x (right-hand side) calculated with $m_c = 1.5$ GeV, $\mu^2 = Q^2 + 20\,\mathrm{GeV}^2$ and CTEQ3 in the $\overline{\mathrm{MS}}$ scheme. From top to bottom the average energy transfer ν is 53, 95 and 168 GeV respectively.

Intrinsic Charm

Proton wavefunction can be expanded as sum over complete basis of quark and gluon states: $|\Psi_p\rangle = \Sigma_m \, |m\rangle \, \psi_{m/p}(x_i, k_{T,i}, \lambda_i)$

$|m\rangle$ are color singlet state fluctuations into Fock components $|uud\rangle$, $|uudg\rangle \cdots |uudc\overline{c}\rangle$

Boost invariant wavefunctions $\psi_{m/p}(x_i, k_{T,i}, \lambda_i)$ depend on $x_i = k_i^+/P^+$ and $k_{T,i}$ the momentum fraction and transverse momentum for each parton. Momentum conservation demands $\Sigma_{i=1}^n x_i = 1$ and $\Sigma_{i=1}^n \vec{k}_{T,i} = 0$, where n is the number of partons in Fock state $|m\rangle$

The intrinsic charm fluctuations can be freed by a soft interaction if the system is probed during the time $\Delta t = 2p_{\rm lab}/M^2_{c\overline{c}}$ that the fluctuations exist

Dominant Fock state configurations have minimal invariant mass, $M^2 = \Sigma_i \, m^2_{T,i}/x_i$, where $m^2_{T,i} = k^2_{T,i} + m^2_i$ is the squared transverse mass of parton i in the state; corresponds to configurations with equal rapidity constituents

Since intrinsic charm quarks have the same rapidity as other partons in the state, their larger mass gives them a higher momentum fraction than the comoving light partons

Light Cone Intrinsic Charm Quark Distribution

Frame-independent Fock state wavefunction

$$\Psi(\vec{k}_{\perp i}, x_i) = \frac{\Gamma(\vec{k}_{\perp i}, x_i)}{m_h^2 - M^2}$$

Vertex function Γ assumed to be slowly varying so the denominator controls the particle distributions; mean k_T^2 used to calculate the x distributions

Probability distribution for n-particle Fock state as a function of x

$$\frac{dP_{\rm ic}}{dx_i \cdots dx_n} = N_n[\alpha_s^2(M_{c\overline{c}})]^2 \; \frac{\delta(1 - \Sigma_{i=1}^n x_i)}{(m_h^2 - \Sigma_{i=1}^n (\widehat{m}_i^2/x_i))^2}$$

N_n is a normalization to total probability for each state; heavy quark limit, $\widehat{m}_c$, $\widehat{m}_{\overline{c}} \gg m_h$, $\widehat{m}_q$

$$\frac{dP_{\rm ic}}{dx_i \cdots dx_n} = N_n[\alpha_s^2(M_{c\overline{c}})]^2 \frac{x_c x_{\overline{c}}}{(x_c + x_{\overline{c}})^2} \; \delta(1 - \sum_{i=1}^n x_i)$$

Finally, in a $|uudc\overline{c}\rangle$ state, $n = 5$ and integration over light quarks and $\overline{c}$ gives

$$c(x) \propto \frac{dP_{\rm ic}(x)}{dx} = \frac{1}{2} N_5 x^2 [\frac{1}{3}(1-x)(1 + 10x + x^2) + 2x(1+x)\ln x]$$

If the intrinsic charm probability is 1%, $N_5 = 36$

Intrinsic Charm Structure Functions

Simplest LO F_2^c, no mass effects $F_2^{(0)}(x) = \frac{8}{9} x c(x)$

Hoffmann and Moore incorporated mass effects: scaling variable, $\xi = 2ax[1 + (1 + 4\rho x^2)^{1/2}]^{-1}$ **where** $\rho = m_p^2/Q^2$, $a = [(1 + 4\lambda)^{1/2} + 1]/2$ **and** $\lambda = m_c^2/Q^2$, $c\overline{c}$ **mass constraint,** $\xi \leq \gamma < 1$, $\gamma = 2a\hat{x}[1 + (1 + 4\rho\hat{x}^2)^{1/2}]^{-1}$ $[c(z, \gamma) = c(z) - zc(\gamma)/\gamma$ **for** $z \leq \gamma$**; 0 otherwise]**

$$F_2^{(0)}(x, Q^2, m_c^2) = \frac{8}{9}\xi c(\xi, \gamma)$$

Generalized operator product expansion to include m_c, m_p **for final LO result**

$$\begin{aligned} F_2^{(0)}(x, Q^2, m_c^2) &= \frac{8x^2}{9(1 + 4\rho x^2)^{3/2}} \left[\frac{(1 + 4\lambda)}{\xi} c(\xi, \gamma) + 3\hat{g}(\xi, \gamma) \right] \\ \hat{g}(\xi, \gamma) &= \frac{2\rho x}{(1 + 4\rho x^2)} \int_\xi^\gamma dt \frac{c(t, \gamma)}{t} \left(1 - \frac{\lambda}{\rho t^2} \right) \left[1 + 2\rho x t + \frac{2\lambda x}{t} \right] \end{aligned}$$

The NLO component of intrinsic F_2^c **is**

$$F_2^{(1)}(x, Q^2, m_c^2) = \frac{8}{9}\xi \int_{\xi/\gamma}^1 \frac{dz}{z} c(\xi/z, \gamma) \sigma_2^{(1)}(z, \lambda)$$

$$\begin{aligned} \sigma_2^{(1)}(z, \lambda) = \frac{2\alpha_s}{3\pi}\delta(1 - z)\Big\{ & 4\ln\lambda - 2 + \sqrt{1 + 4\lambda} L + \frac{(1 + 2\lambda)}{\sqrt{1 + 4\lambda}} [3L^2 + 4L + 4\mathrm{Li}_2(-d/a) + 2L\ln\lambda - 4L\ln(1 + 4\lambda) + 2\mathrm{Li}_2(d^2/a^2)] \Big\} + \frac{\alpha_s}{3\pi} \frac{1}{(1 + 4\lambda z^2)^2} \\ \times \Big\{ & \frac{1}{[1 - (1 - \lambda)z]^2} [(1 - z)(1 - 2z - 6z^2 + 8z^4) + 6\lambda z(1 - z)(3 - 15z - 2z^2 + 8z^3) + 4\lambda^2 z^2 (8 - 77z + 65z^2 - 2z^3) + 16\lambda^3 z^3 (1 - 21z + 12z^2) \\ & - 128\lambda^4 z^5] - \frac{2\hat{L}}{\sqrt{1 + 4\lambda z^2}} [(1 + z)(1 + 2z^2) - 2\lambda z(2 - 11z - 11z^2) - 8\lambda^2 z^2 (1 - 9z)] - \frac{8z^4(1 + 4\lambda)^2}{(1 - z)_+} - \frac{4z^4(1 + 2\lambda)(1 + 4\lambda)^2 \hat{L}}{\sqrt{1 + 4\lambda z^2}(1 - z)_+} \Big\} \end{aligned}$$

$$\hat{L} = \ln \left[\frac{4\lambda z[1 - (1 - \lambda)z]}{(1 + 2\lambda z + \sqrt{1 + 4\lambda z^2})^2} \right]$$

Intrinsic F_2^c for EMC Analysis

IC contribution at higher Q^2 and x than EC, NLO range is not as broad as LO

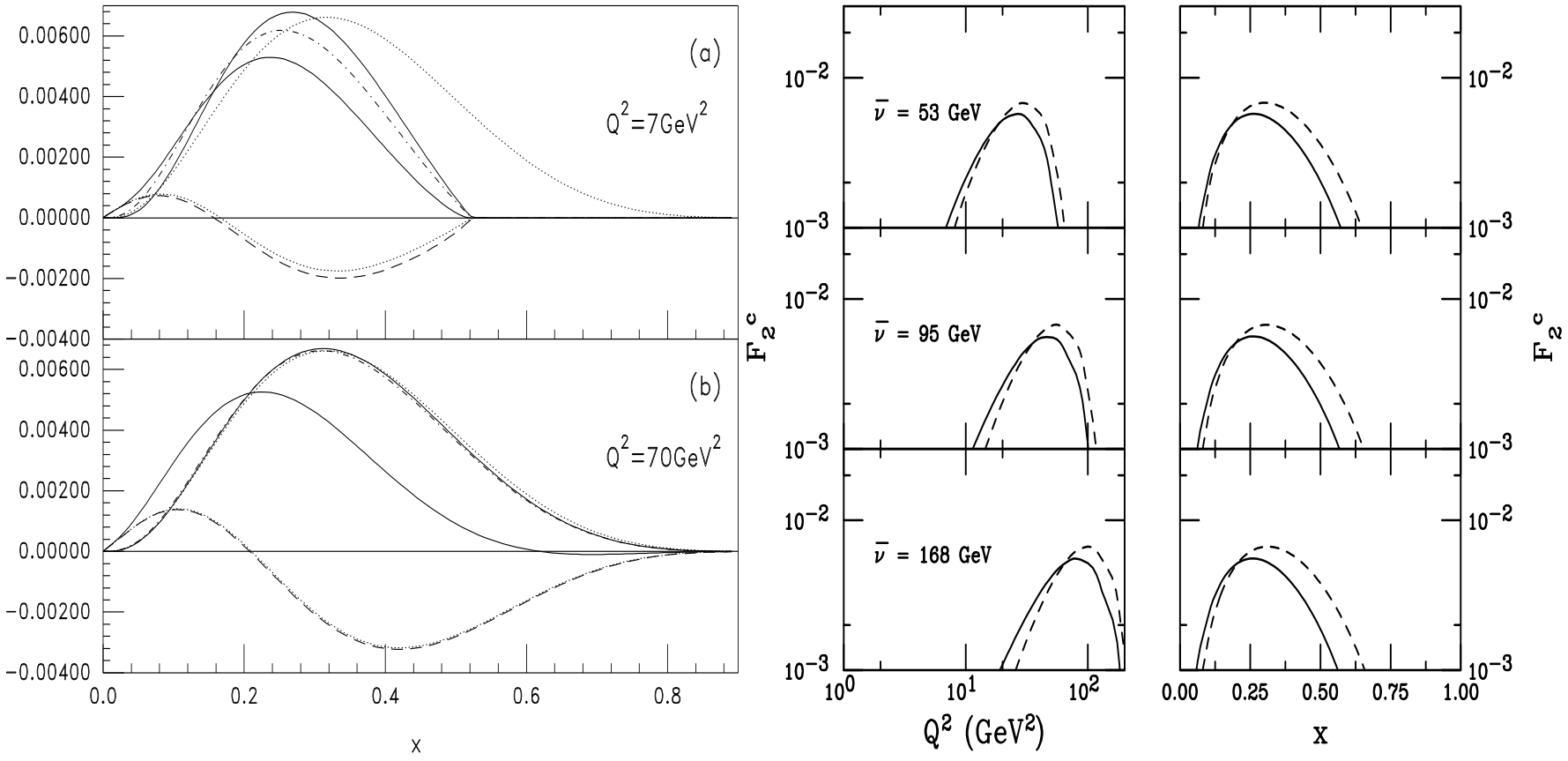

Figure 7: (Left) The IC contributions to the structure function $F_2(x, Q^2, m_c^2)$. At LO we show the massless result (upper dotted), the ξ-scaling result (dot-dashed) and the full kinematically corrected formula (upper solid). The full NLO correction (lower dotted) and the leading-log approximation (dashed) are also shown, along with the sum of the LO and NLO full results (lower solid). The results are given for $Q^2 = 7$ (a) and 70 (b) GeV^2. From Harris, Smith and RV. (Right) The intrinsic charm structure function used in the EMC analysis as a function of Q^2 (left-hand side) and x (right-hand side). From top to bottom the average energy transfer ν is 53, 95 and 168 GeV respectively. The full LO (dashed) and NLO (solid) results are shown.

Comparison to EMC Data

Normalization of EC and IC components free parameters in fit to EMC charm data (Harris, Smith and R.V.)

$$F_2^c(x,Q^2,m_c^2) = \alpha\, F_2^{c,\mathrm{EC}}(x,Q^2,m_c^2) + \beta\, F_2^{c,\mathrm{IC}}(x,Q^2,m_c^2)$$

α gives measure of NNLO correction, β is based on a 1% IC normalization

Uncertainties are for 95% confidence level; most significant result is at highest $\overline{\nu}$

	$\bar{\nu} = 53$ GeV		$\bar{\nu} = 95$ GeV		$\bar{\nu} = 168$ GeV	
PDF	α	β	α	β	α	β
CTEQ3	0.95 ± 0.64	0.36 ± 0.58	1.20 ± 0.13	0.39 ± 0.31	1.27 ± 0.06	0.92 ± 0.53
MRS G	1.02 ± 0.69	0.34 ± 0.58	1.38 ± 0.15	0.32 ± 0.32	1.47 ± 0.07	0.79 ± 0.53
GRV94	1.15 ± 0.77	0.33 ± 0.58	1.45 ± 0.16	0.34 ± 0.31	1.48 ± 0.08	0.88 ± 0.53

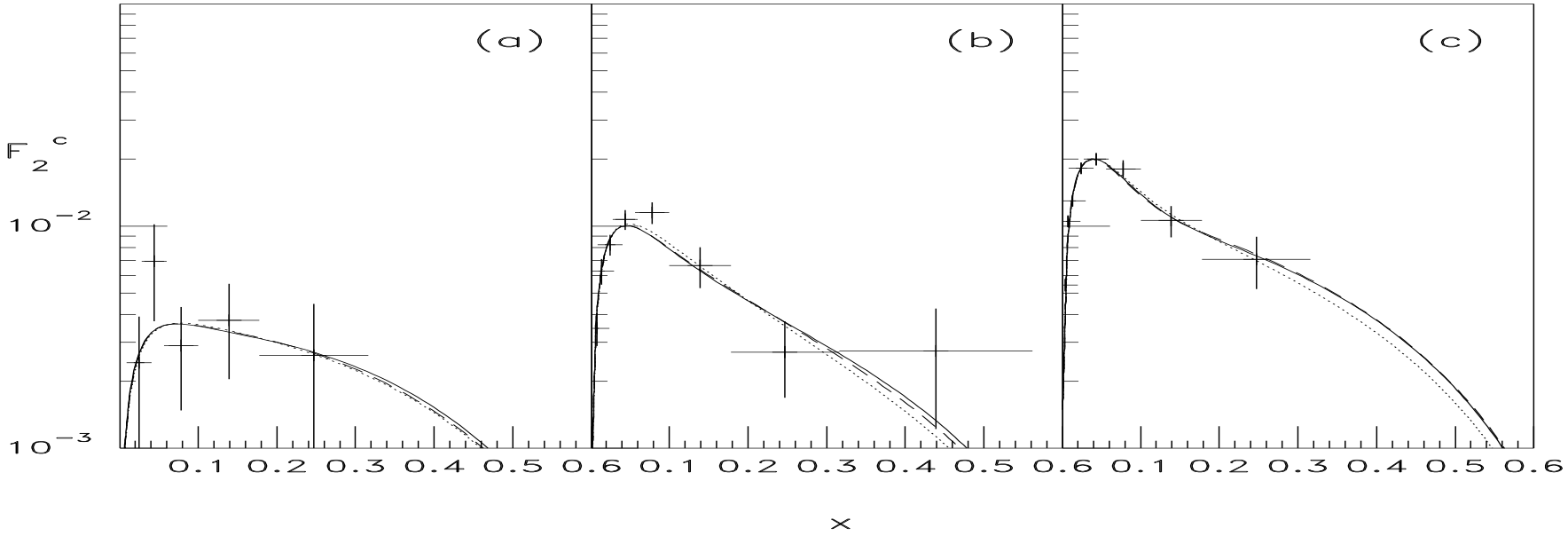

Figure 8: The sum of the EC and IC structure functions, weighted by the parameters α and β, are compared to the EMC F_2^c for $\overline{\nu} = 53$ (a), 95 (b) and 168 (c) GeV. The results are shown for CTEQ3 (solid), MRS G (dotted) and GRV98 (dashed) as a function of x. (From Harris, Smith and R.V..)

Global Analysis with Intrinsic Charm by Pumplin *et al.*

Performed global analysis including the presence of nonperturbative charm in the parton densities

Pumplin *et al.* refer to extrinsic charm as *radiatively generated charm*, the charm parton density is completely determined by the gluon and light quark parameters and evolution

Their work is first general global analysis to include: coherent treatment of nonzero quark masses in pQCD and experimental inputs that constrain the charm degree of freedom (they use HERA data, not EMC data)

Compare three different scenarios:

- **Light cone formalism of Brodsky *et al.***

$$c(x) = \overline{c}(x) = Ax^2[6x(1+x)\ln x + (1-x)(1+10x+x^2)]$$

- **Meson cloud picture with $c(x) \neq \overline{c}(x)$**

$$\begin{aligned} c(x) &= Ax^{1.897}(1-x)^{6.095} \\ \overline{c}(x) &= \overline{A}x^{2.511}(1-x)^{4.929} \\ 0 &= \int_0^1 dx[c(x) - \overline{c}(x)] \end{aligned}$$

- **Charm distribution is sea-like, similar to light flavor sea**

$$c(x) = \overline{c}(x) \propto \overline{d}(x) + \overline{u}(x)$$

Results of Global Fits

Fits based on CTEQ6.5 analysis without IC

Includes quark mass effects in DIS a la Collins along with relevant HERA I data in addition to other data used in global fits

IC allowed within each scenario characterized by $\langle x \rangle_{c+\overline{c}}$ at $\mu_0 = 1.3$ GeV,

$$\langle x \rangle_{c+\overline{c}} = \int_0^1 dx\, x\, [c(x) + \overline{c}(x)] \tag{1}$$

Global χ^2 insensitive to $\langle x \rangle_{c+\overline{c}} < 0.01$, little evidence to confirm or refute IC

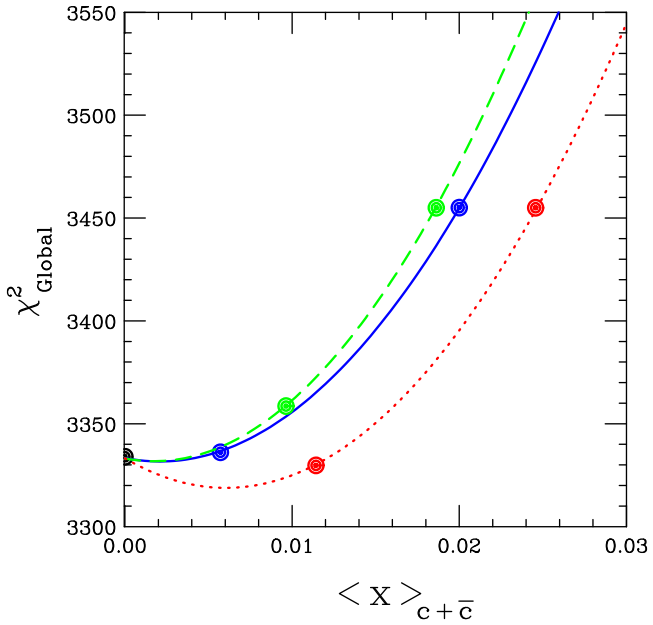

Figure 9: Goodness of fit for global analyses including IC as a function of $\langle x \rangle_{C+\overline{c}}$ for the light-cone formalism of Brodsky *et al.* (solid), the meson-cloud model (dashed); and sea-like (dotted). The lower dots correspond to candidate fits, 0.057% for Brodsky *et al.*, 0.96% for the meson cloud and 1.1% for sea-like IC. The upper dots are the most marginal fits in the different scenarios, 2% for Brodsky *et al.*, 1.9% for the meson cloud and 2.4% for sea-like. [From Pumplin *et al.*]

Pumplin Results

Extracted Brodsky *et al.* result is similar to that obtained by Harris *et al.* without incorporating a global analysis

Meson cloud IC gives harder distribution for the Λ_c-like charm quark than the $\overline{D}$ meson anticharm quark

Sea-like IC results in an enhancement over all x

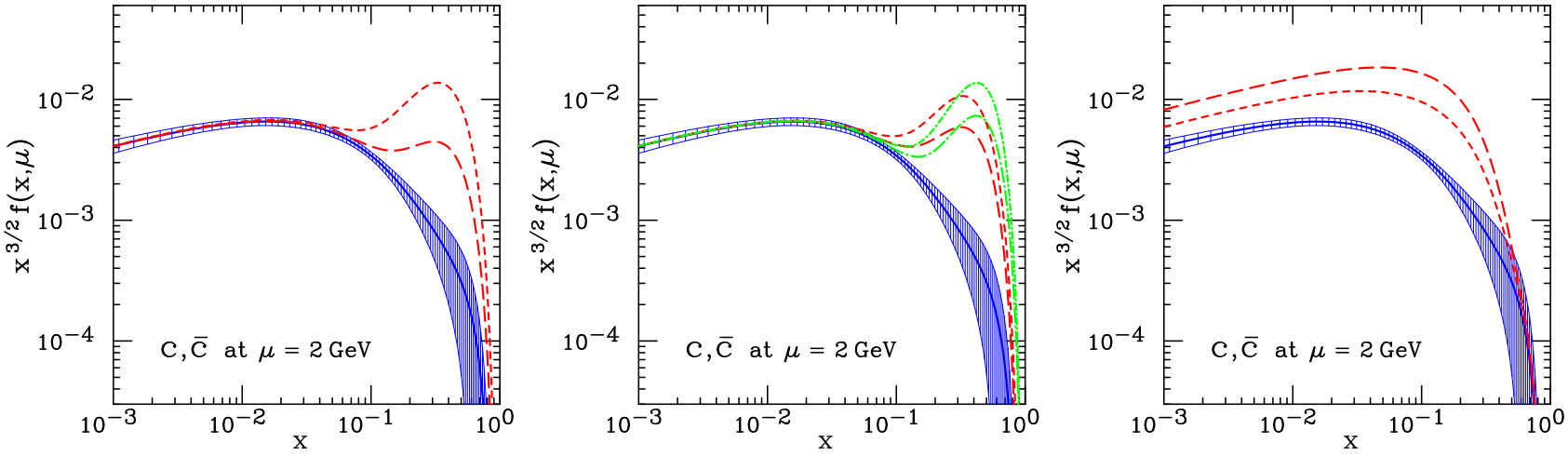

Figure 10: The three IC scenarios at scale $\mu = 2$ GeV. The left-hand panel shows the Brodsky *et al.* light-cone result; the central shows the meson cloud result (the baryonic component is that with the peak at higher $\langle x \rangle_{c+\bar{c}}$); and the right panel shows the sea-like IC shape. The long-dashed and short dashed curves correspond to the minimum and maximum values of $\langle x \rangle_{c+\bar{c}}$ in each scenario. The solid curve and shaded region show the central value and uncertainty from CTEQ6.5, which contains no IC. [From Pumplin *et al.*]

Scale Evolution of Charm Distribution

QCD evolution makes charm distribution softer at higher scales

IC component is dominant at large x and remains different from evolution without IC, even at large scales

Scale of x axis is linear in $x^{1/3}$ to enhance large x region

IC should have observable consequences in experiments that can access the large x region

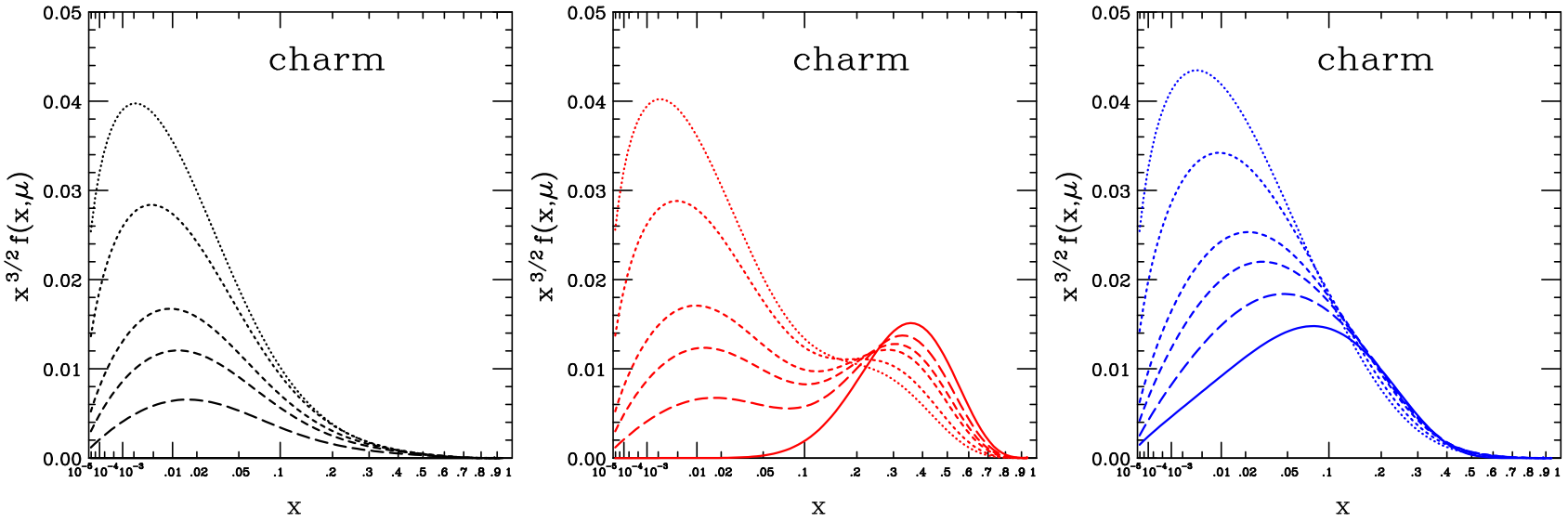

Figure 11: The scale evolution of the charm distribution without IC (left); with the Brodsky *et al.* light-cone result (center); and the sea-like IC shape (right). The results are shown for $\mu = 1.3$ (solid), 2, 3.16, 5, 20 and 100 (dotted) GeV in each case. [From Pumplin *et al.*]

Light Cone IC Leads to Interesting Observable Consequences

IC states can either fragment, like normal leading-twist factorization of charm production or coalesce into charm mesons and baryons

Charm hadrons formed by IC coalescence are produced with much higher x_F than at leading twist, these are leading charm hadrons

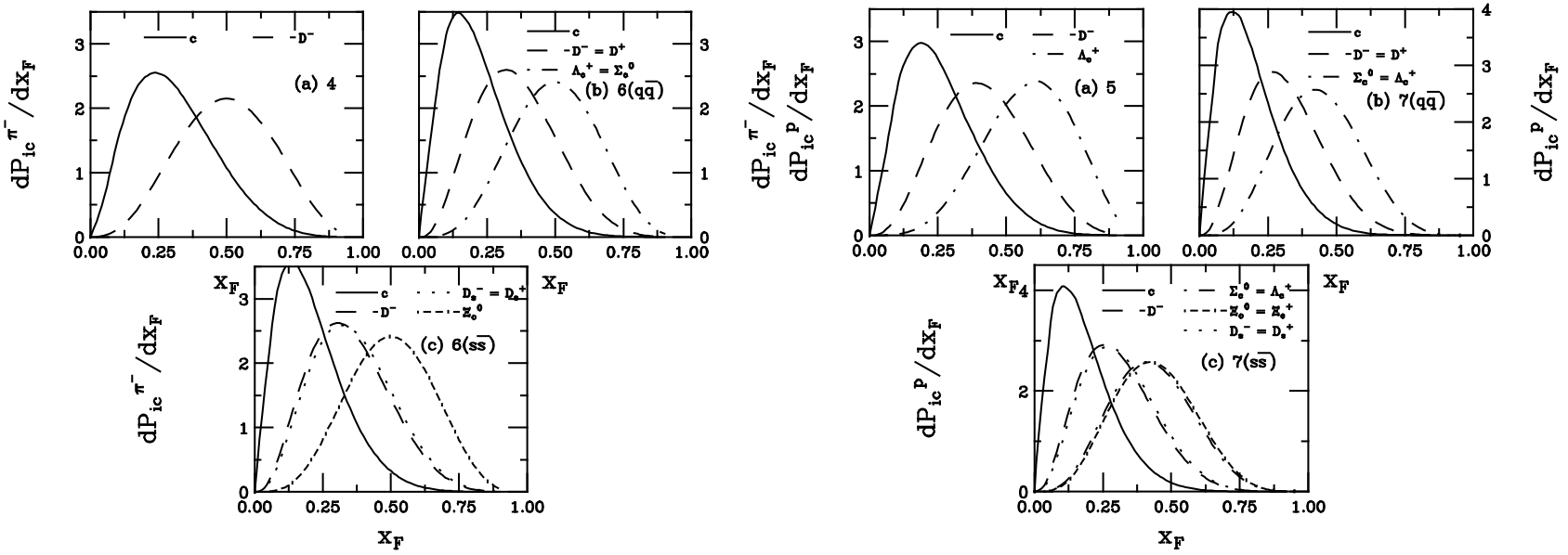

Figure 12: Charm hadron production in the intrinsic charm model with a π^- (left) and proton (right) projectile. The probability distributions, $(1/P_{\rm ic}^n)(dP_{\rm ic}^n/dx_H)$, for uncorrelated fragmentation and coalescence with a π^- projectile (left) are given for the minimal 4-particle Fock state (a) and for the 6-particle Fock states with light quarks $q = u$, d (b) and with strange quarks (c). The probability distributions, $(1/P_{\rm ic}^n)(dP_{\rm ic}^n/dx_H)$, for uncorrelated fragmentation and coalescence with a proton projectile (right) are given for the minimal 5-particle Fock state (a) and for the 7-particle Fock states with light quarks $q = u$, d (b) and with strange quarks (c). The solid curve in each case is the charm quark distribution which also serves as the hadron distribution for independent fragmentation. The other curves are the probability distributions for hadron production by coalescence, including: D^- (dashed), Λ_c^+ (dot-dashed), Ξ_c^0 (dot-dash-dashed) and D_s^- (dotted). If the shape of the probability distribution is the same for any two hadrons (such as the Σ_c^0 and the Λ_c^+ in (b)) in a configuration, it is indicated. [From Gutierrez and RV.]

Asymmetries Observed Between Leading and Nonleading Charm

Asymmetries mostly observed in fixed target $\pi^- A$ interactions

Should be observable with protons too, fewer measurements with poorer statistics

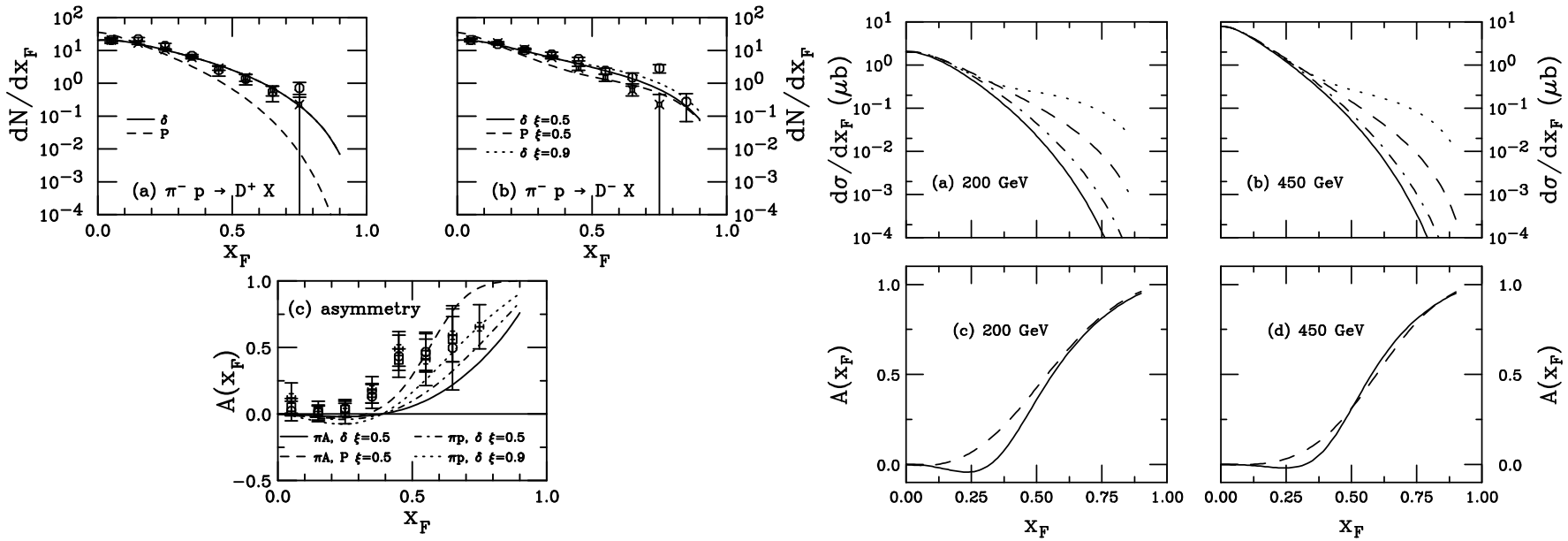

Figure 13: (Left) results for (a) nonleading charm and (b) leading charm distributions in $\pi^- p$ interactions at 340 GeV and (c) the asymmetry are compared with the WA82 (circles) and E769 (stars) data. The combined asymmetry from both experiments is also shown (squares). The calculations are with GRV LO distributions using delta-function (solid) and Peterson function (dashed) fragmentation with the intrinsic charm contributions to nonleading and leading charm production. The dotted curve in (b) shows the leading D distribution with $\xi = 0.9$ (weight factor of coalescence relative to fragmentation). The dot-dashed curve is shows the prediction of fusion with final-state coalescence. In (c), the dashed curve is calculated with the Peterson function and the solid curve with delta-function fragmentation. Both are averaged over nuclear target. The dot-dashed curve uses delta-function fragmentation and a proton target. The dotted curve shows the leading contribution calculated with $\xi = 0.9$ for a proton target. [From Brodsky and RV.] (Right) Predictions of the energy dependence of charm hadron production by a proton beam on lead targets. The curves in (a) and (b) illustrate the dependence of leading charm on the projectile energy. The fusion curve (solid) includes no IC while the other curves assume $P_{\rm ic} = 0.31\%$. They are D^- (dashed), D^+ (dot-dashed) and Λ_c (dotted). The D^-/D^+ (solid) and Λ_c/D^- (dashed) asymmetries are shown at 200 GeV (c) and 450 GeV (d).

Possible Observable Consequences at RHIC

Brodsky and Lansberg computed CSM quarkonium rapidity distribution at LO and NLO

Also included a LO contribution due to $cg \to J/\psi c$ enhanced by IC, diagram (b) below

Such an additional J/ψ production mechanism could be observed via a charm jet opposite in azimuth to the J/ψ

Azimuthal correlation would be sensitive to the charm distribution in the proton

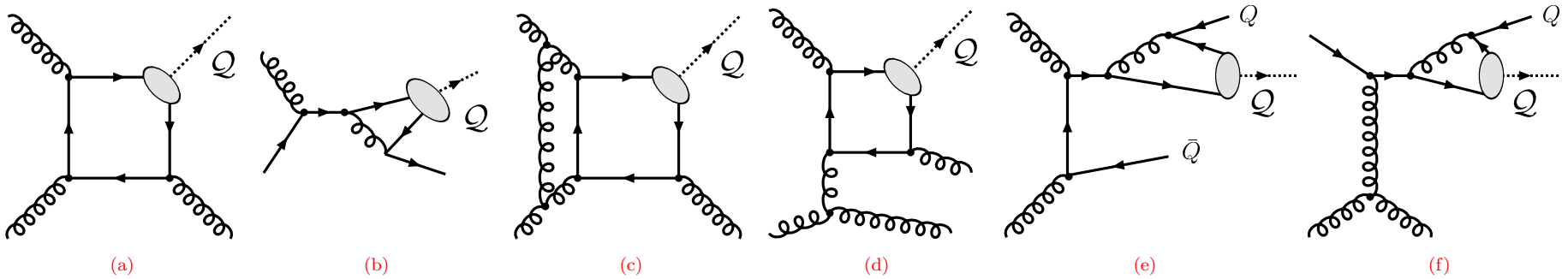

Figure 14: Representative diagrams contributing to ${}^3S_1$ quarkonium (denoted $\mathcal{Q}$) hadroproduction via color singlet channels at order α_s^3 (a,b) and α_s^4 (c,d,e,f). The quark and antiquark attached to the ellipses are assumed to be on shell with zero relative velocity v.

PHENIX Results Can Be Described Within CSM (+ IC)

Brodsky and Lansberg calculated direct J/ψ (no χ_c or ψ' feed down) in the LO ($\mathcal{O}(\alpha_s^3)$) and NLO (up to $\mathcal{O}(\alpha_s^4)$) CSM

Obtained uncertainty bands by varying charm quark mass and scale

NLO CSM in good agreement with PHENIX J/ψ data (scaled to obtained the direct cross section)

Including cg diagrams with sea-like IC improves agreeement; $J/\psi + c$ final state is significant fraction of total J/ψ in this approach

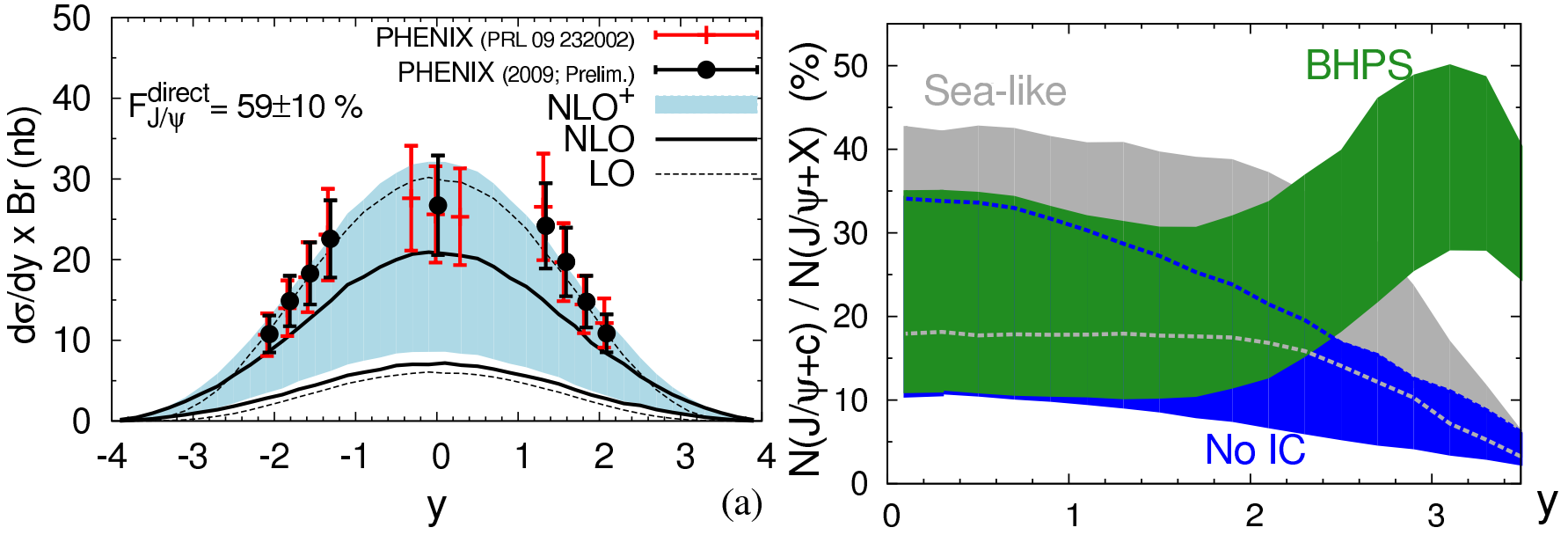

Figure 15: (Left) The rapidity distribution, $B d\sigma^{direct}_{J/\psi}/dy$ from PHENIX multiplied by the fraction of direct J/ψ production compared to the CSM at LO (α_s^3) by gg fusion only (thin-dashed lines), at NLO (up to α_s^4) by gg and qg fusion only (thick-solid lines) and the sum "NLO + cg fusion" with the sea-like IC, denoted NLO$^+$ (light-blue band). (Right) Fraction of J/ψ produced in association with a single c-quark ($gc \to J/\psi c$) relative to the direct yield (NLO$^+$) as a function of y_ψ and for no IC, sea-like and Brodsky *et al.* (BHPS).

What If We Make the Nucleus a Target?

Medium Effects Important with Nuclear Target

Nuclear effects often parameterized as

$$\sigma_{pA} = \sigma_{pp} A^{\alpha} \qquad \alpha(x_F, p_T)$$

For $\sqrt{s_{NN}} \leq 40$ GeV and $x_F > 0.25$, α decreases strongly with x_F – only low x_F effects probed by SPS and RHIC rapidity coverage

Possible cold matter effects

- **Nuclear Shadowing — initial-state effect on the parton distributions affecting total rate, important as a function of y/x_F**
- **Energy Loss — initial-state effect, elastic scatterings of projectile parton before hard scattering creating quarkonium state, need to study Drell-Yan production to get a handle on the strength when shadowing included**
- **Intrinsic Charm — initial-state effect, if light-cone models correct, should only contribute to forward production, assumed to have different A dependence than normal J/ψ production**
- **Absorption — final-state effect, after $c\overline{c}$ that forms the J/ψ has been produced, pair breaks up in matter due to interactions with nucleons**

Nuclear Modifications of the Parton Densities

Shadowing Parameterizations On The Market

EKS98: K. J. Eskola, V. J. Kolhinen and P. V. Ruuskanen, Nucl. Phys. B 535 (1998) 351 [arXiv:hep-ph/9802350]; K. J. Eskola, V. J. Kolhinen and C. A. Salgado, Eur. Phys. J. C 9 (1999) 61 [arXiv:hep-ph/9807297].

nDS: D. de Florian and R. Sassot, Phys. Rev. D 69, 074028 (2004) [arXiv:hep-ph/0311227].

HKN: M. Hirai, S. Kumano and T. H. Nagai, Phys. Rev. C 70, 044905 (2004) [arXiv:hep-ph/0404093].

FGS: L. Frankfurt, V. Guzey and M. Strikman, Phys. Rev. D 71 (2005) 054001 [arXiv:hep-ph/0303022].

EPS08: K. J. Eskola, H. Paukkunen and C. A. Salgado, JHEP 0807, 102 (2008) [arXiv:0802.0139 [hep-ph]].

EPS09: K. J. Eskola, H. Paukkunen and C. A. Salgado, JHEP 0904 (2009) 065 [arXiv:0902.4154 [hep-ph]].

Differences Between Eskola *et al* Sets

EKS98 Simple parameterization for all A; leading order analysis only; GRV LO set used for proton PDFs; single set; **no χ^2 analysis performed;** $2.25 \leq Q^2 \leq 10^4$ **GeV**^{2}; $10^{-6} < x < 1$

EPS08 Simple parameterization for all A; leading order analysis only; CTEQ61L set used for proton PDFs; single set; **χ^2 analysis uses forward BRAHMS data from RHIC to maximize gluon shadowing;** $1.69 \leq Q^2 \leq 10^6$ **GeV**^{2}; $10^{-6} < x < 1$

EPS09 Available for select A values; LO and NLO sets available based on CTEQ61L and CTEQ6M respectively; **χ^2 analysis done at both LO and NLO;** calling routine similar to other sets but now there are 31, 15 above and 15 below the central set; **no longer use BRAHMS data**

If χ^2-minimized set of parameters, $\{a_0\}$, gives best estimate of nPDFs, work in a basis $\{z\}$ that diagonializes covariance matrix, errors in nPDFs computed within 90% confidence criteria, $\Delta\chi^2 = 50$

Upper and lower uncertainties in any observable X can be computed using the prescription

$$(\Delta X^+)^2 \approx \sum_k \left[\max\left\{X(S_k^+) - X(S^0), X(S_k^-) - X(S^0), 0\right\}\right]^2$$
$$(\Delta X^-)^2 \approx \sum_k \left[\max\left\{X(S^0) - X(S_k^+), X(S^0) - X(S_k^-), 0\right\}\right]^2$$

In all cases, when A, x or Q^2 are outside the range of validity, the last value is returned, *e.g.* if $x < 10^{-6}$ value at $x = 10^{-6}$ is given

Q^2 Dependence of EPS09 – Constrains Gluon

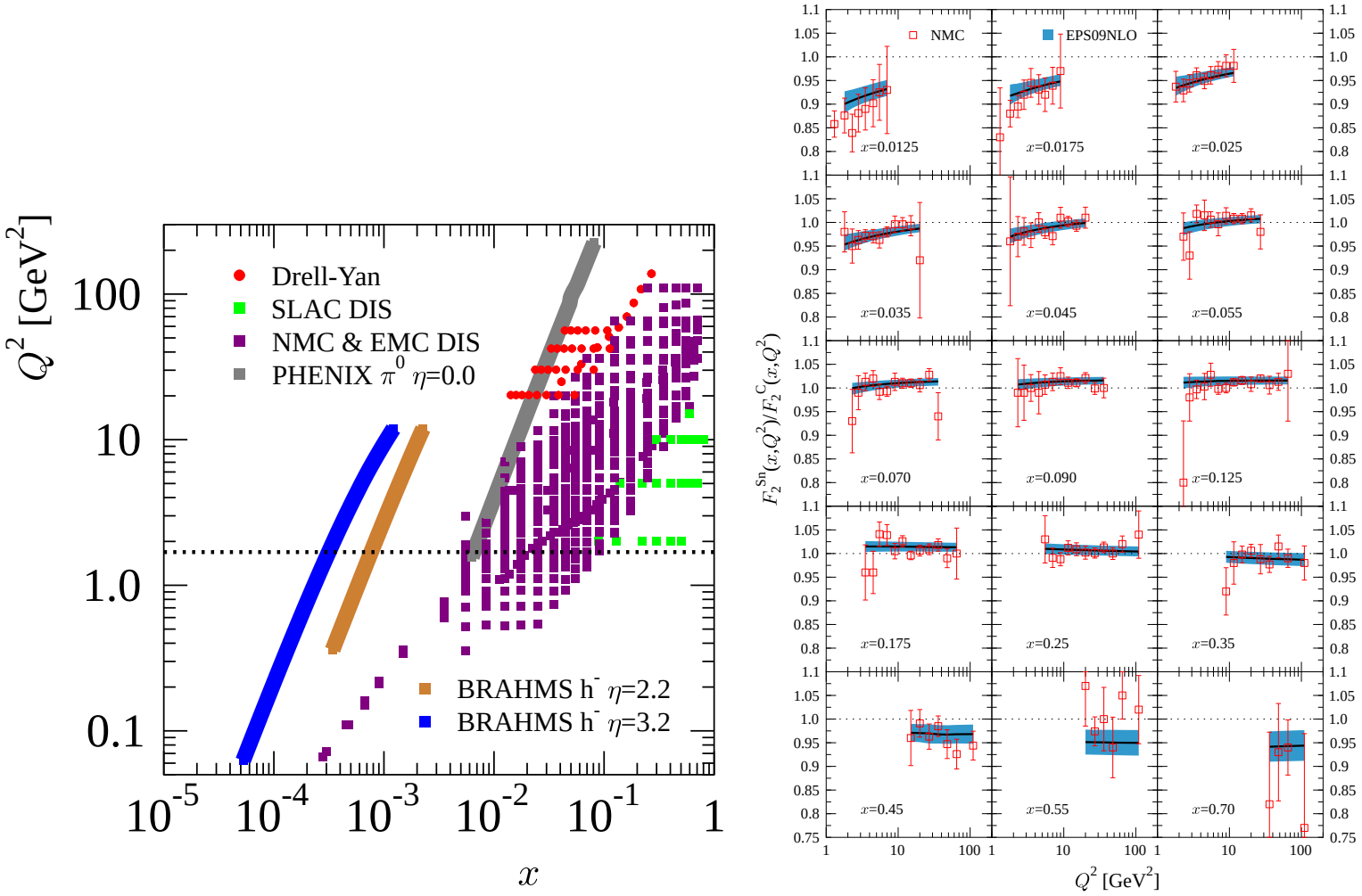

Figure 16: **Left: initial gluon distributions at $Q_0^2 = 1.4$ GeV^2. Right: evolution of gluon distributions for several fixed values of x shows that the effect of the nonlinear terms vanishes as Q^2 increases.**

x Dependence of EPS09

Note that the width of the uncertainty band can be bigger than any individual ratio since the errors added in quadrature

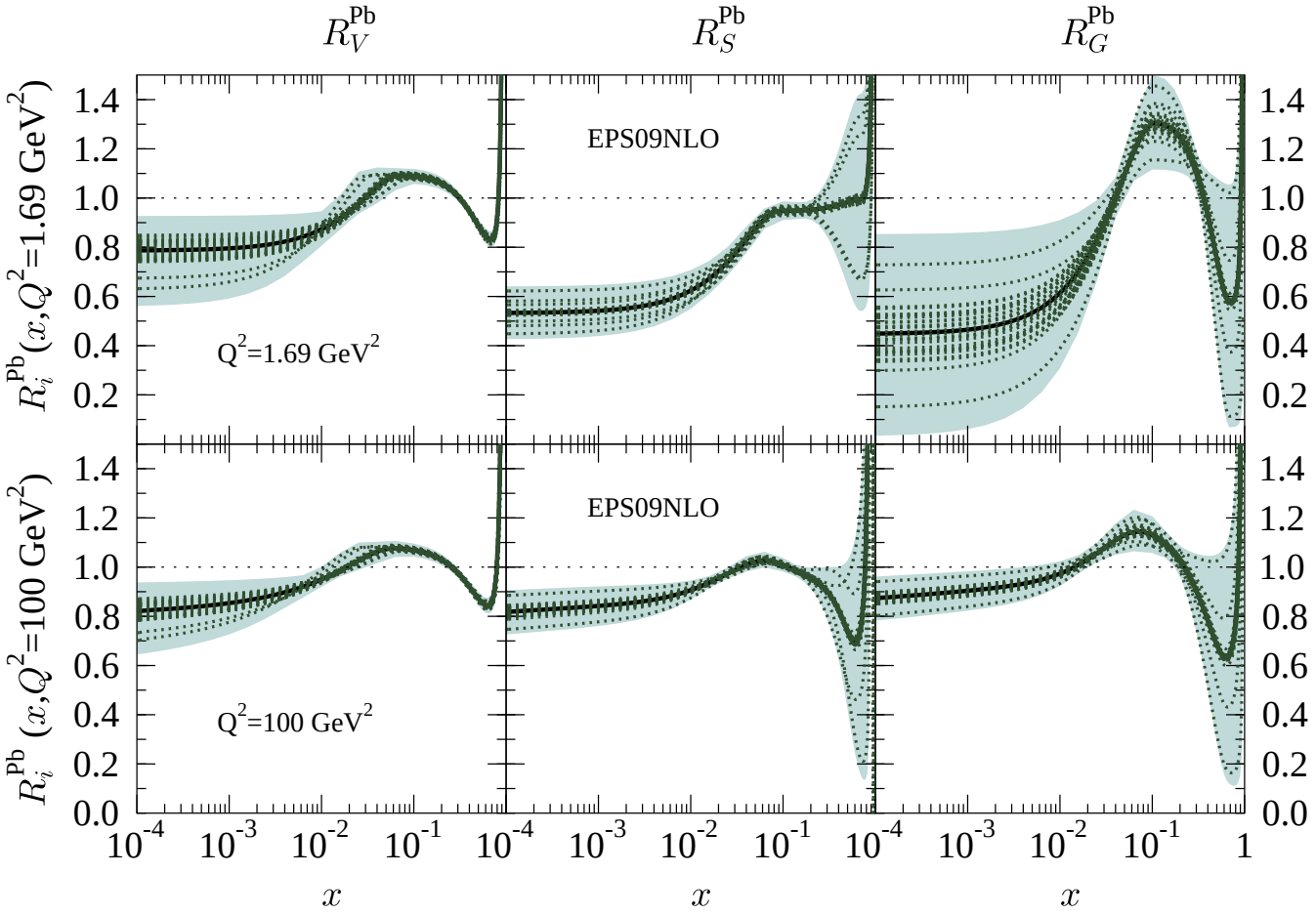

Figure 17: **Left: initial gluon distributions at $Q_0^2 = 1.4$ GeV^2. Right: evolution of gluon distributions for several fixed values of x shows that the effect of the nonlinear terms vanishes as Q^2 increases.**

Comparison of LO and NLO nDS nPDFs

While the magnitude of the absolute cross sections may differ at LO and NLO, the effect of shadowing is, by design, the same at LO and NLO

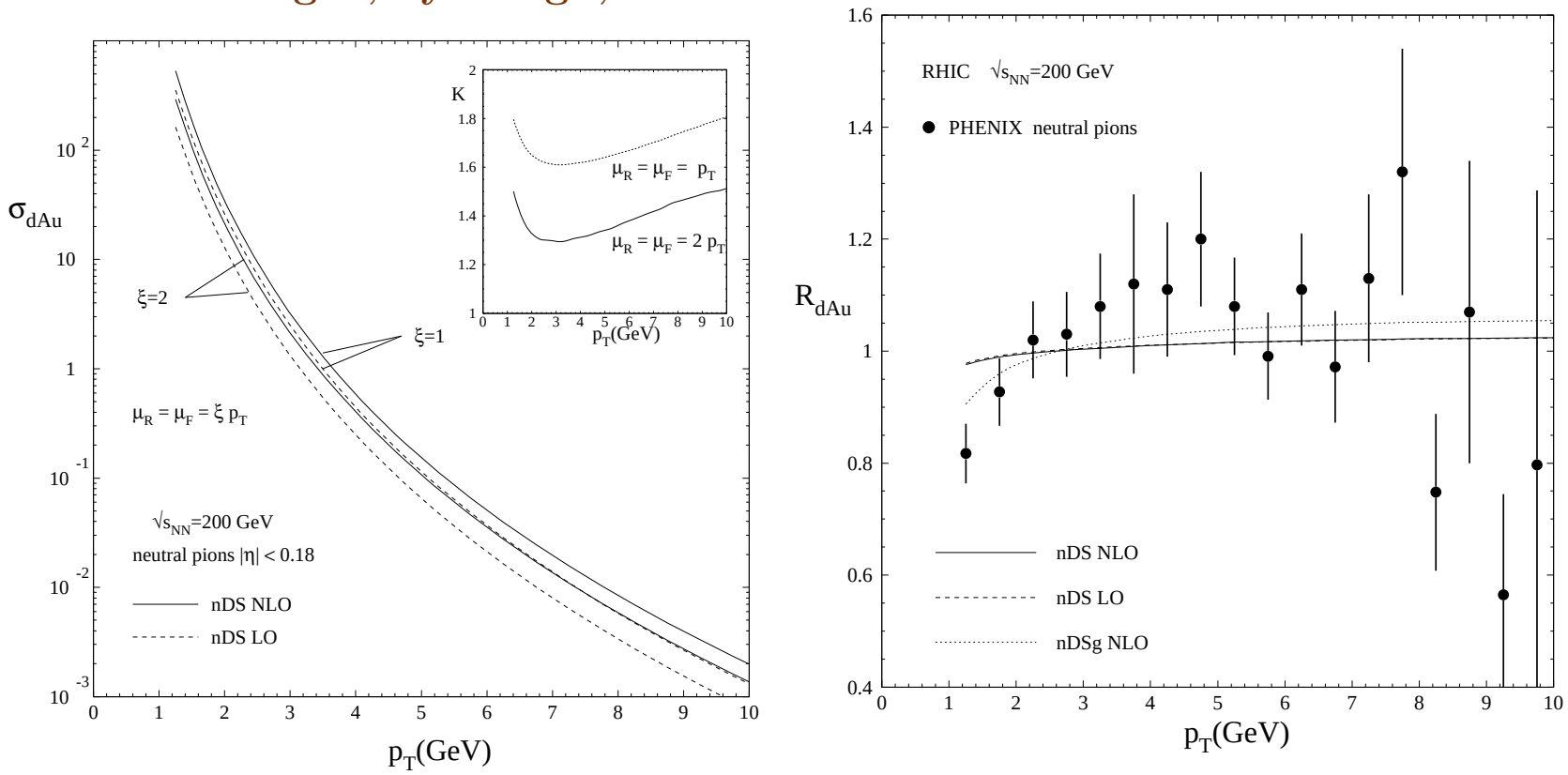

Figure 18: **Left: The π^0 cross section in d+Au collisions at $\sqrt{s_{NN}} = 200$ GeV at LO and NLO. Right: The LO and NLO calculations of $R_{\rm dAu}$.**

Comparing Shadowing Parameterizations: x Dependence

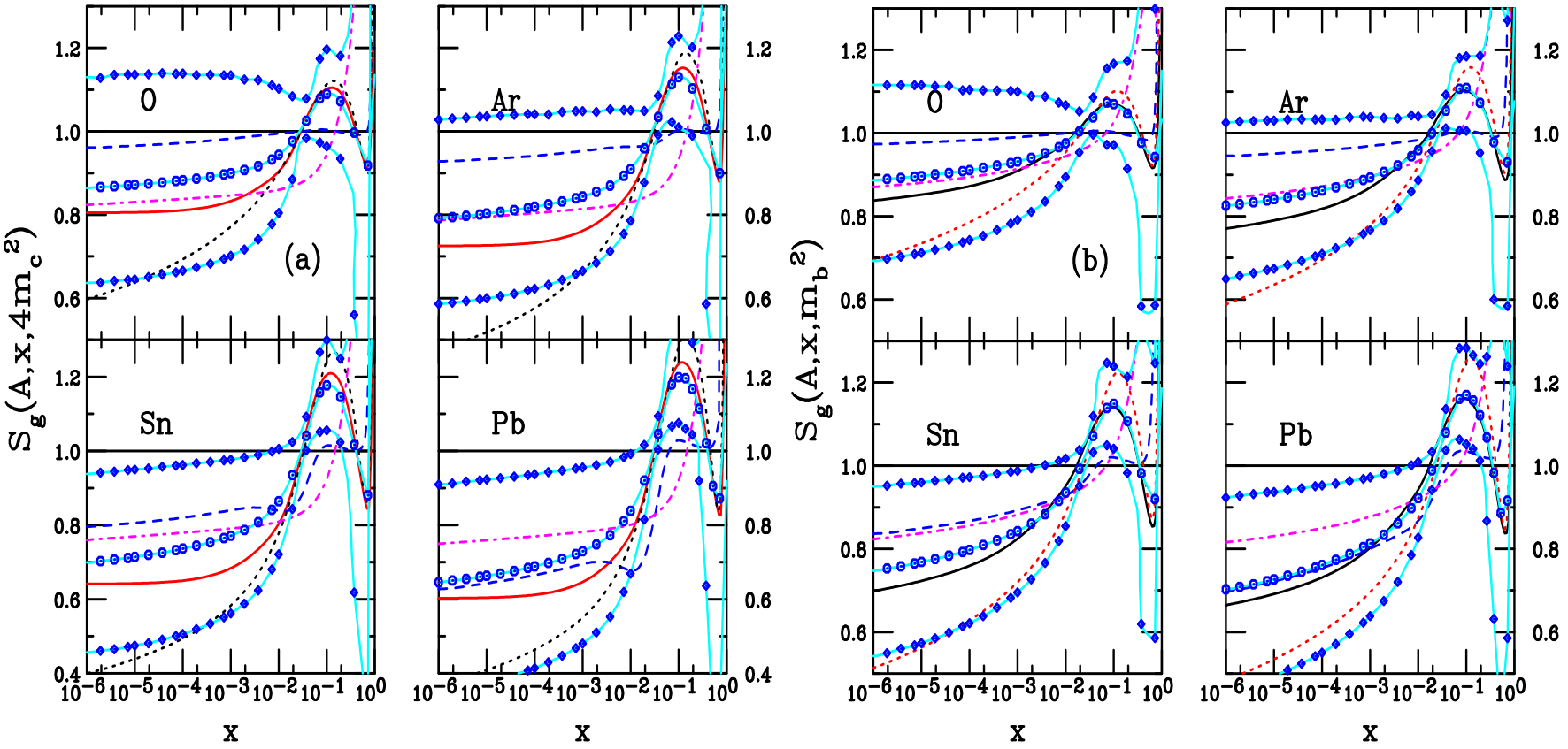

Figure 19: **Comparison of EKS98 (red), nDSg (blue), HKN (green), EPS08 (magenta), and EPS09 (cyan, with symbols) gluon shadowing parameterizations for J/ψ (left) and Υ (right) production scales with A =O, Ar, Sn and Pb.**

Can't J/ψ Constrain Nuclear Gluon Density?

Probably Not

To constrain gluon density using the J/ψ, you also must constrain other cold matter effects, including energy loss, IC and absorption

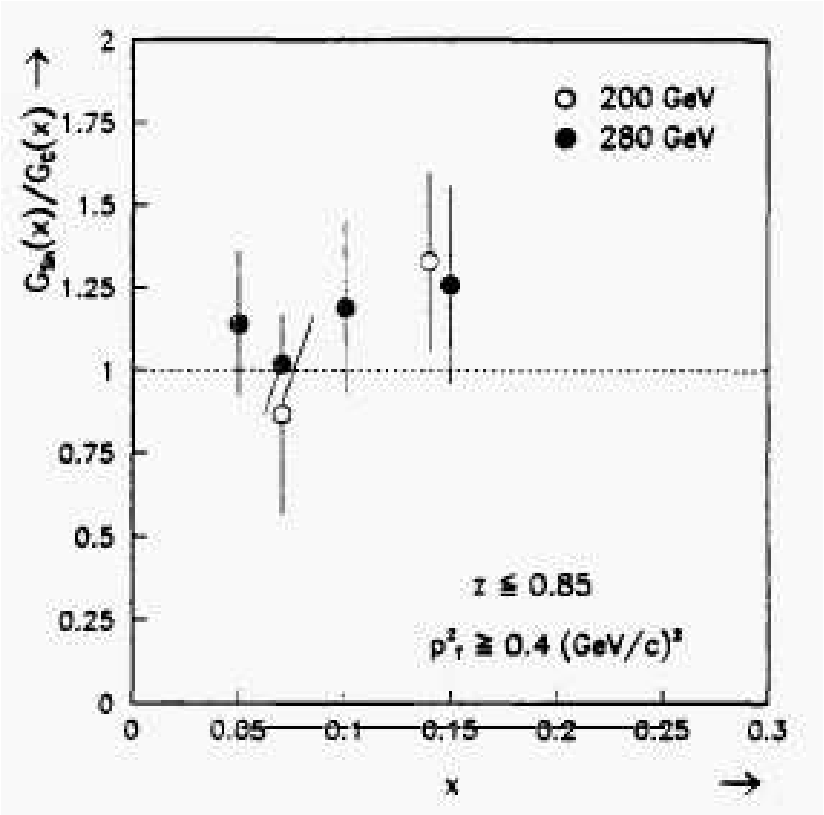

Figure 20: **Ratio of gluon distributions in Sn and C targets extracted from J/ψ production by NMC.**

Kinematics of J/ψ Production at Midrapidity

pW/pp ratios of J/ψ production calculated with EKS98 and no final-state absorption

Left: Dependence on $\sqrt{s_{NN}}$ at $x_F = 0$, energies of typical data indicated

Right: Dependence on x_F for three different energies; antishadowing peak narrows closer to $x_F \sim 0$; shadowing stronger at forward x_F

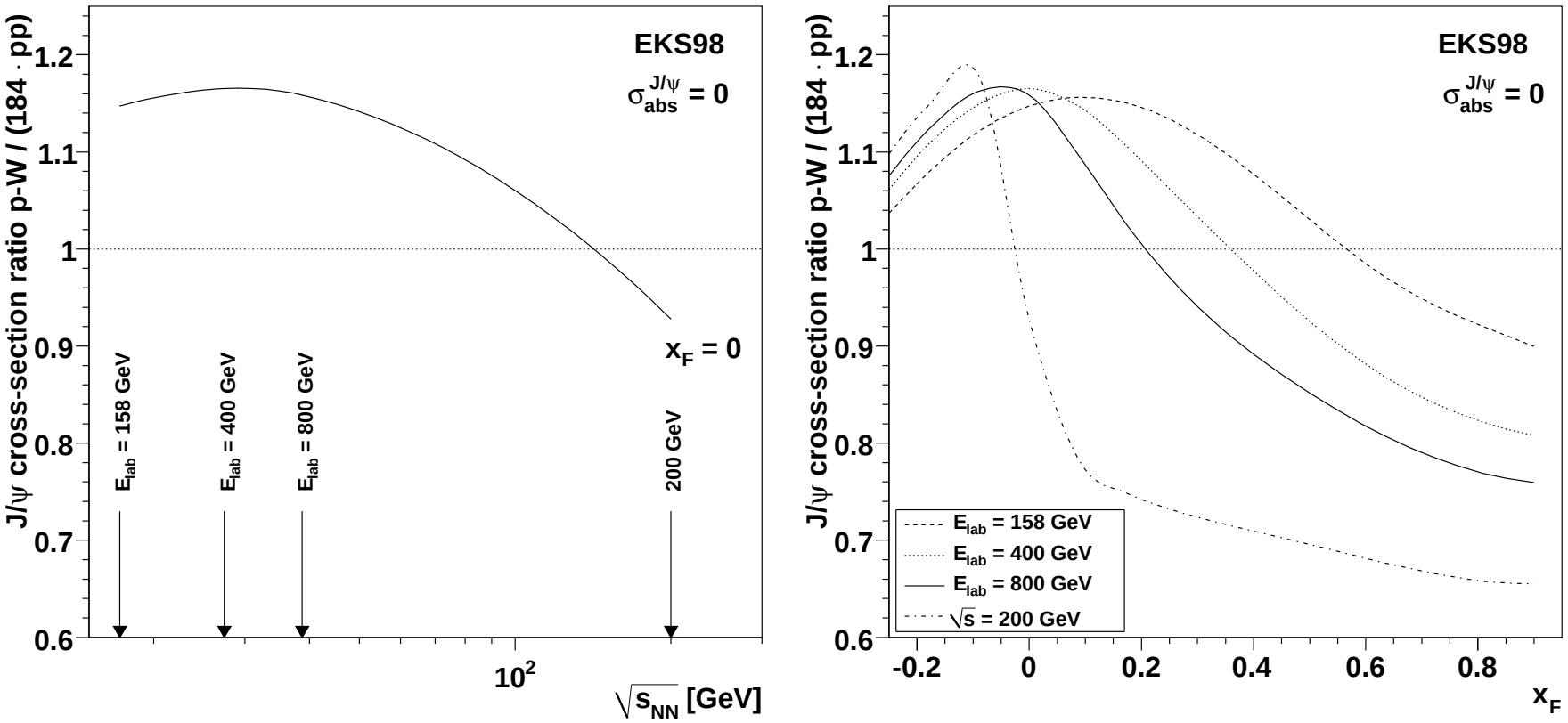

Figure 21: Changes induced by the nuclear modifications of the PDFs on the J/ψ production cross section per nucleon, in pW collisions, with EKS98, as a function of collision energy at $x_F = 0$ (left) and as a function of x_F at three proton beam energies (right). [Lourenço, RV, Wöhri]

Final-State Absorption

Quarkonium Absorption by Nucleons

Woods-Saxon nuclear density profiles typically used

$$\begin{aligned}\sigma_{pA} &= \sigma_{pN}\int d^2b \int_{-\infty}^{\infty} dz\, \rho_A(b,z) S_A^{\rm abs}(b) \\ &= \sigma_{pN}\int d^2b \int_{-\infty}^{\infty} dz\, \rho_A(b,z) \exp\left\{-\int_z^{\infty} dz' \rho_A(b,z')\sigma_{\rm abs}(z'-z)\right\}\end{aligned}$$

Note that if $\rho_A = \rho_0$, $\alpha = 1 - 9\sigma_{\rm abs}/(16\pi r_0^2)$

The value of $\sigma_{\rm abs}$ **depends on the parameterization of** σ_{pA} **– Glauber, hard sphere,** A^α **etc. (shown by NA50)**

Initial-state shadowing only recently taken into account at SPS energies

Feed down to J/ψ **from** χ_c **and** ψ' **decays not always included, should dictate that**

$$\sigma_{pA} = \sigma_{pN}\int d^2b\, [0.6 S_{\psi,\,\rm dir}(b) + 0.3 S_{\chi_{cJ}}(b) + 0.1 S_{\psi'}(b)]$$

Each charmonium state should interact with a different asymptotic absorption cross section, not yet included; formation time dependence yet to be incorporated

The χ_c A **dependence remains unknown**

A Dependence of J/ψ and ψ' Not Identical

Color octet mechanism suggested that J/ψ and ψ' A dependence should be identical — Supported by large uncertainties of early data

More extensive data sets (NA50 at SPS, E866 at FNAL) show clear difference at midrapidity [NA50 ρL fit gives $\Delta\sigma = \sigma^{\psi'}_{\rm abs} - \sigma^{J/\psi}_{\rm abs} = 4.2 \pm 1.0$ mb at 400 GeV, 2.8 ± 0.5 mb at 450 GeV for absolute cross sections]

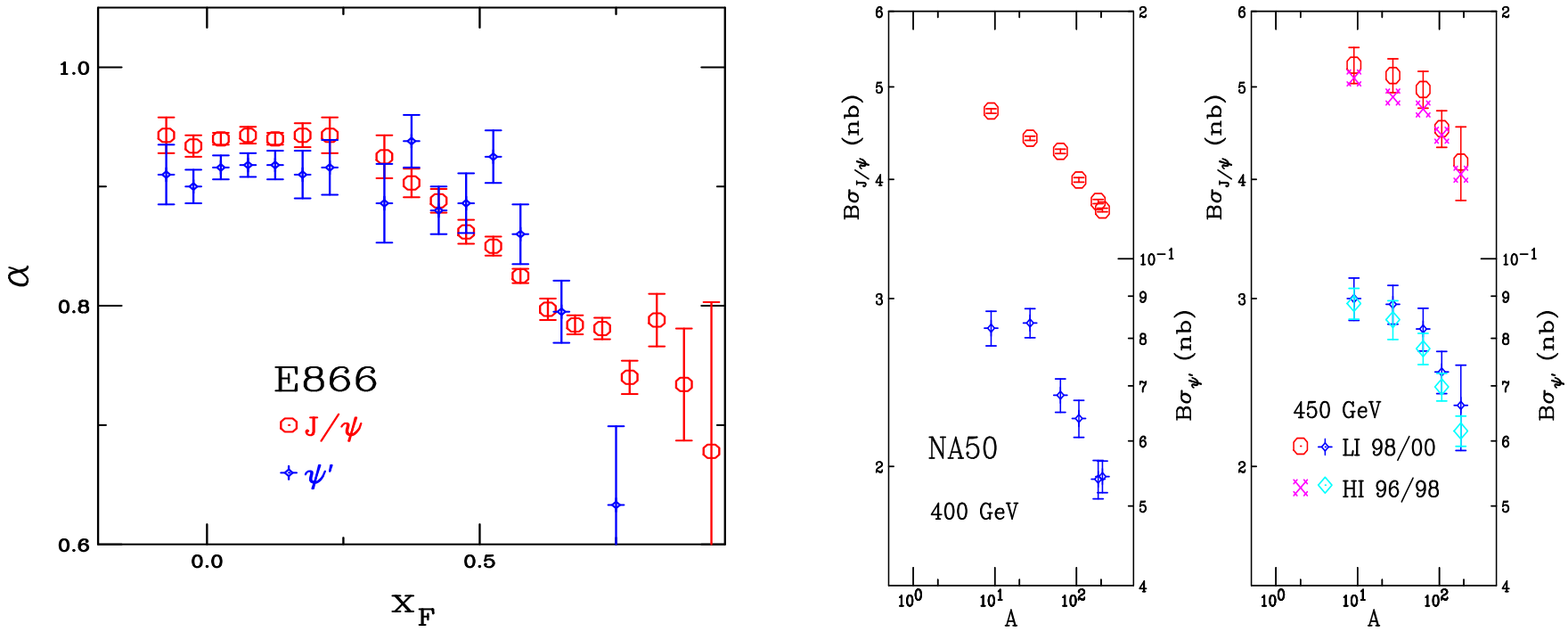

Figure 22: **The J/ψ A dependence (left) as a function of x_F at FNAL ($\sqrt{s_{NN}} = 38.8$ GeV) and (right) and a function of A at the SPS (NA50 at $p_{\rm lab} = 400$ and 450 GeV) for J/ψ and ψ' production.**

Some Results and Some Speculations

Interplay of Shadowing and Absorption

Depending on x values probed, shadowing can enhance or reduce absorption cross section needed to describe data

Absorption alone always gives less than linear A dependence ($\alpha < 1$)

For SPS energies, $17.3 \leq \sqrt{s} \leq 29$ GeV, rapidity range covered is in EMC and antishadowing region, $\alpha > 1$ with no absorption

Adding shadowing to SPS absorption calculations requires a larger absorption cross section to maintain agreement with data

For $\sqrt{s} \geq 38$ GeV, x in shadowing regime, thus $\alpha < 1$ with shadowing alone in forward region, reducing absorption cross section needed at midrapidity

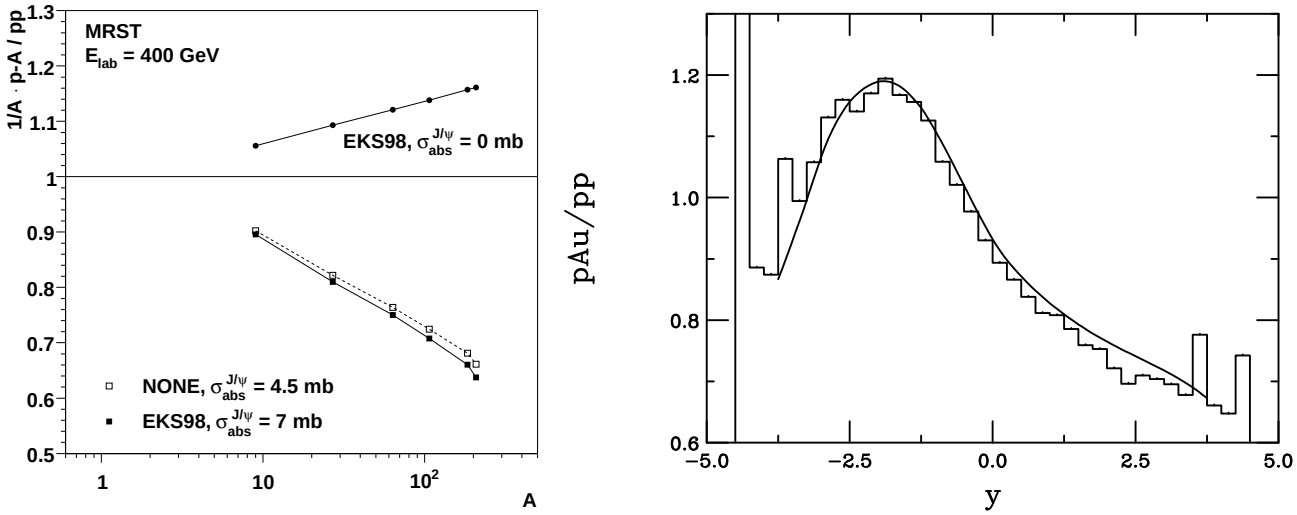

Figure 23: **(Left) Illustration of the interplay between shadowing and absorption. [C. Lourenco, H. K. Woehri and RV, JHEP 0902 (2009) 014.] (Right) Comparison of LO and NLO shadowing ratios.**

Fit $\sigma_{\rm abs}^{J/\psi}$ to Data and Extrapolate to Other Energies

Asymmetric Gaussians used to fit $x_F < 0.25$ region of E866 and HERA-B data

Shapes at other energies determined by fits, magnitude adjusted to data: $\sigma_{\rm abs}^{J/\psi}$ seems to decrease with energy

Even with no shadowing effects included (left-hand side), there seems to be a systematic decrease of the absorption cross section with energy

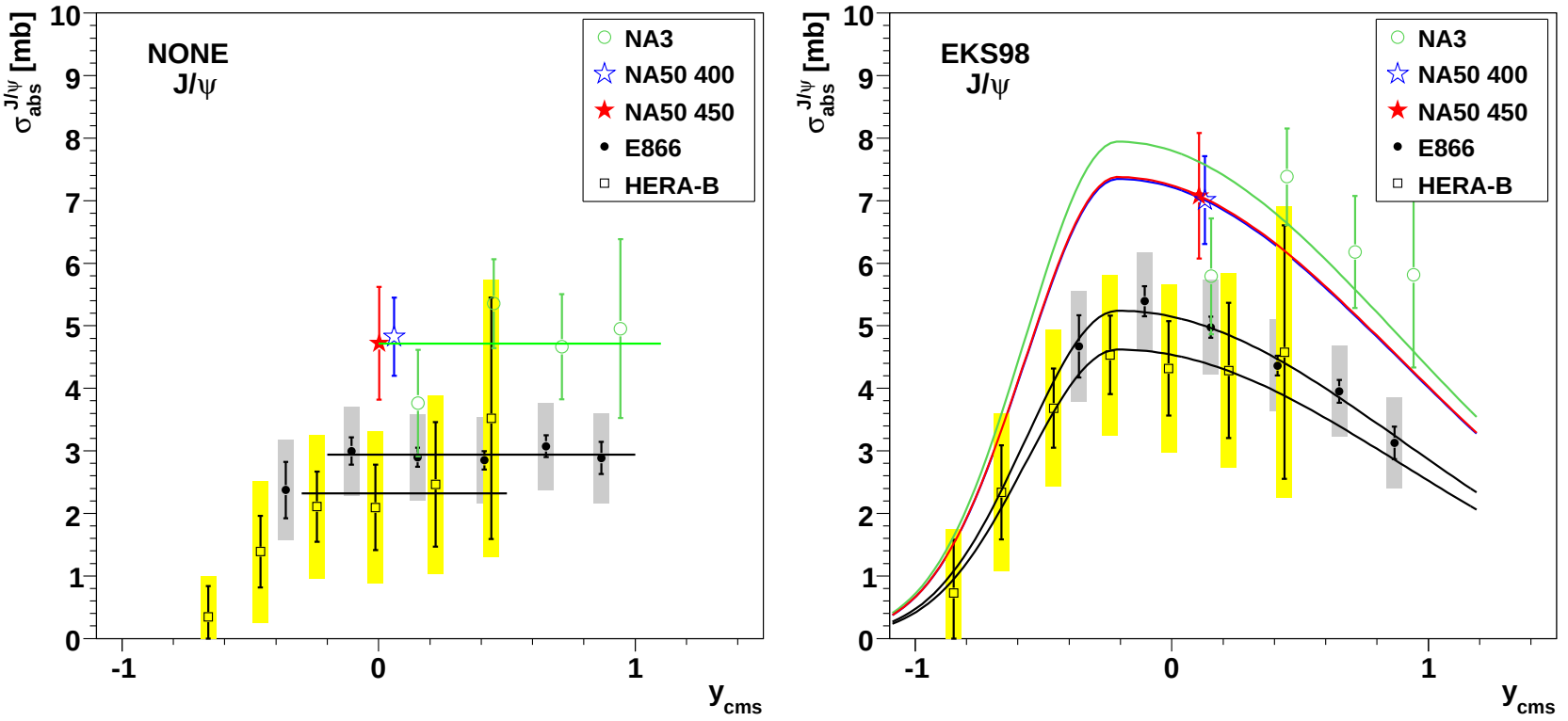

Figure 24: Dependence of $\sigma_{\rm abs}^{J/\psi}$ on $y_{\rm cms}$ for all available data sets. The shape of the curves is fixed by the E866 and HERA-B data. [Lourenço, RV, Wöhri] Left: Assuming no shadowing effects on the PDFs. Right: Including EPS98 shadowing.

Quantifying Energy Dependence of $\sigma_{\rm abs}^{J/\psi}$

$\sigma_{\rm abs}^{J/\psi}(y_{\rm cms}=0)$ **decreases with** $\sqrt{s_{NN}}$

$\sigma_{\rm abs}^{J/\psi}(y_{\rm cms}=0)$ **extrapolated to 158 GeV is significantly larger than measured at 450 GeV, underestimating "normal nuclear absorption" in SPS heavy-ion data**

Calculations confirmed by NA60 pA **measurements at 158 GeV (QM09)**

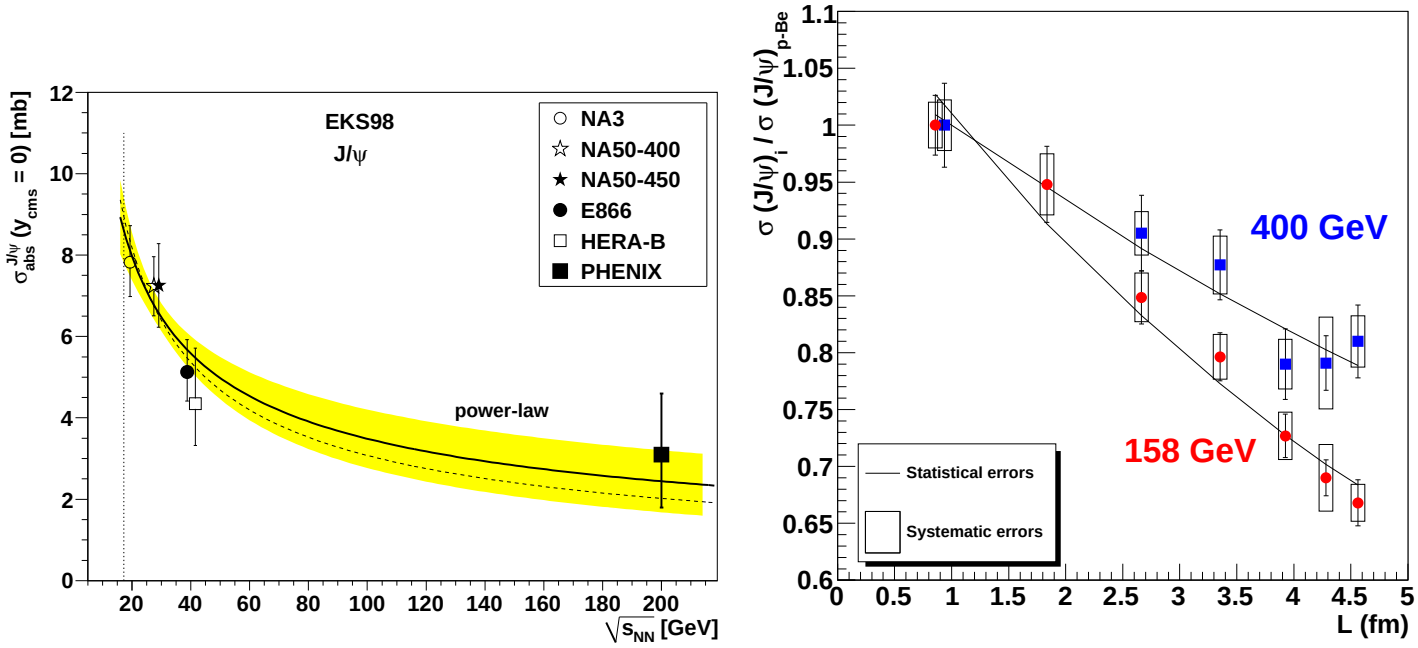

Figure 25: (Left) Energy dependence of $\sigma_{\rm abs}^{J/\psi}$ at $y=0$, using the EKS98 shadowing parameterization with the CTEQ61L parton densities. [?, ?]. The NA3, NA50, E866, and HERA-B points show the $y=0$ interpolated values while the PHENIX point represents the value integrated within $|y|<0.35$. The solid line and the error band reflect a power law fit of all the data points while the dashed line only fits the fixed target data. The vertical dotted line indicates the energy of the Pb+Pb and In+In collisions at the CERN SPS. [Modified from Lourenço, RV, Wöhri]. (Right) The J/ψ cross section ratios for pA collisions at 158 GeV (circles) and 400 GeV (squares), as a function of L, the mean thickness of nuclear matter traversed by the J/ψ. [Arnaldi, Cortese, Scomparin]

x_F Dependence of $\sigma_{\rm abs}^{J/\psi}$ Shows Holes in Our Understanding

Forward x_F ($y_{\rm cms}$) data more complex: strongly increased absorption in this region

NA60 data begin to rise at lower x_F than do higher energy results from E866 and PHENIX, behavior at lower energy suggests effect unrelated to gluon saturation

Such strong effects can't come from any of the shadowing parameterizations shown before; we are investigating effects of energy loss but first need to set the possible quark energy loss level in NLO DY production, work in progress with C. Lorenco, H. Wöhri and P. Faccioli

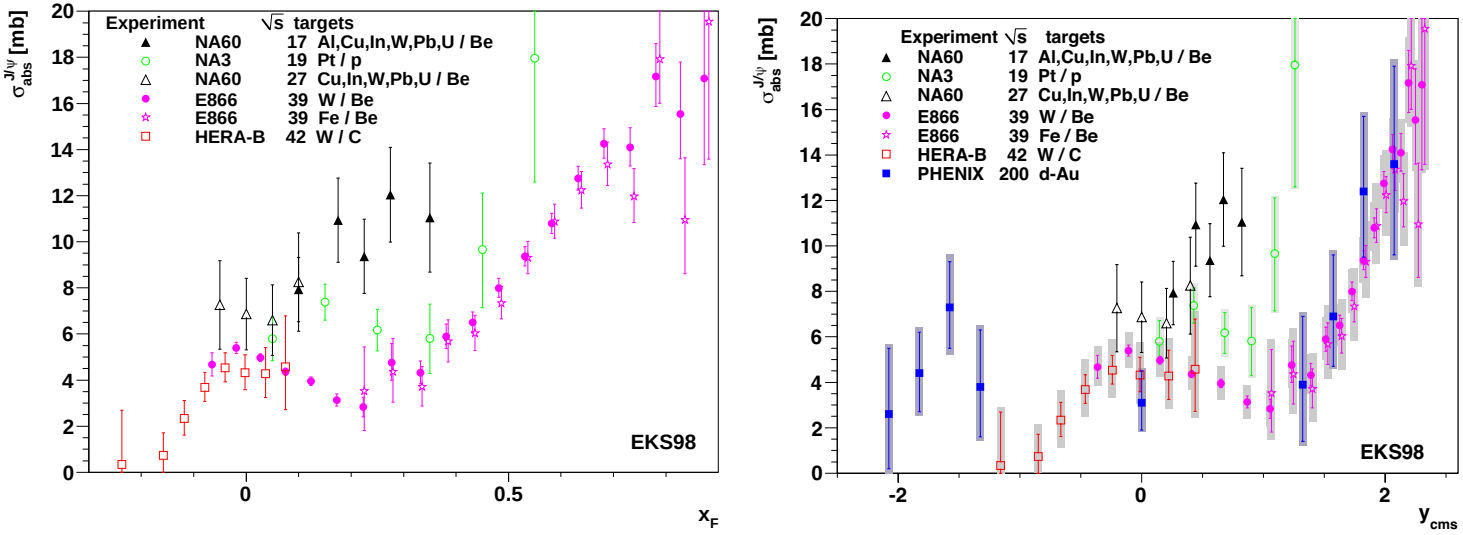

Figure 26: Left: The x_F dependence of $\sigma_{\rm abs}^{J/\psi}$ for incident fixed-target energies from 158, 200, 400, 450, 800 and 920 GeV obtained using the EKS98 shadowing parameterization. Right: The same results as above but as a function of center-of-mass rapidity $y_{\rm CMS}$. The absorption cross sections extracted from the preliminary PHENIX results at $|y_{\rm CMS}| > 0$ and the central rapidity result are also included. [Plots made by Hermine Wöhri with PHENIX data from Tony Frawley.]

Shadowing is Not Enough

Rather wide range of EPS09 uncertainty reduced in ratios; clearly initial-state shadowing must be supplemented by other mechanisms like energy loss and IC

Results shown with energy loss implemented as $x'_{1\,p} = x_1/(1-\epsilon_p)^{(N_{\rm coll}-1)}$ where $x_{1\,p}$ is the initial projectile parton momentum fraction; x_1 is mometum fraction in the hard scattering; $\epsilon_g \approx (9/4)\epsilon_q$, other parameterizations give different shapes

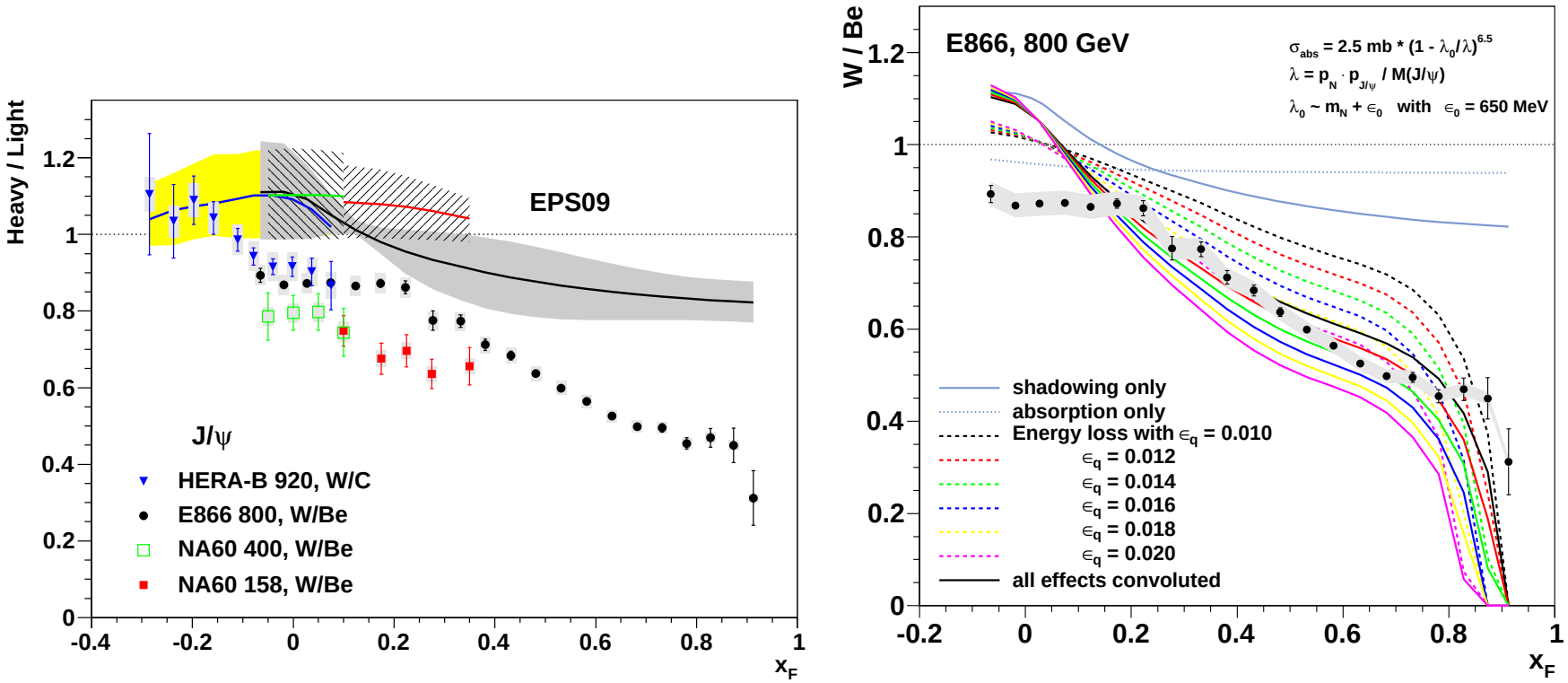

Figure 27: (Left) The W/Be ratios in fixed-target interactions. (Right) Convolution of shadowing, absorption with various levels of initial-state quark energy loss compared to the E866 data.

What About IC?

Include IC in addition to other effects, compare to E866 data

GM refers to $\Delta x_1 \propto x_1$ while BH represents with $\Delta x_1 \propto 1/x_1$

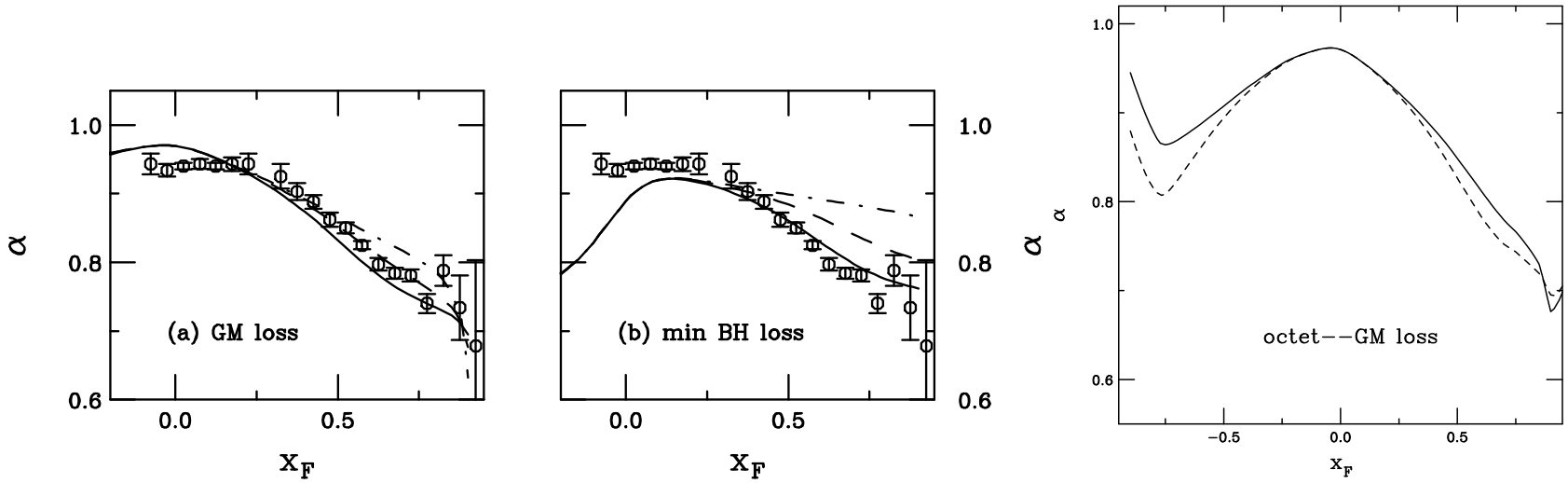

Figure 28: (Left)The effective probability of intrinsic charm is varied for pure octet production with (a) GM loss and (b) the minimum BH loss. The curves represent an effective intrinsic charm probability of 1% (solid), 0.31% (dashed) and 0% (dot-dashed). (Right) The value of α (W/C) for the GM loss model with 1% (dashed) and 0.3% (solid) at 920 GeV.

Summary .

- CEM agrees well with RHIC data; useful tool for studying cold nuclear matter effects .
- CSM with IC also agrees with RHIC J/ψ rapidity distribution
- IC could be distinguished at large x by studying asymmetries in exclusive/semi-exclusive production if light-cone picture is correct
- Data seem to suggest absorption cross section decreases with $\sqrt{s_{NN}}$ and increases at forward x_F modulo other effects, inconsistent with saturation
- Difficult to use J/ψ to extract nuclear gluon distribution in nDIS without better understanding of all cold matter effects